

GRAVITATIONAL ENCOUNTERS AND THE EVOLUTION OF GALACTIC NUCLEI. III. ANOMALOUS RELAXATION

DAVID MERRITT

Department of Physics and Center for Computational Relativity and Gravitation, Rochester Institute of Technology, Rochester, NY 14623

Draft version October 16, 2018

ABSTRACT

This paper is the third in a series presenting the results of direct numerical integrations of the Fokker-Planck equation for stars orbiting a supermassive black hole (SBH) at the center of a galaxy. The algorithm of Paper II included diffusion coefficients that described the effects of random (“classical”) and correlated (“resonant”) relaxation. In this paper, the diffusion coefficients of Paper II have been generalized to account for the effects of “anomalous relaxation,” the qualitatively different way in which eccentric orbits evolve in the regime of rapid relativistic precession. Two functional forms for the anomalous diffusion coefficients are investigated, based on power-law or exponential modifications of the resonant diffusion coefficients. The parameters defining the modified coefficients are first constrained by comparing the results of Fokker-Planck integrations with previously-published N -body integrations. Steady-state solutions are then obtained via the Fokker-Planck equation for models with properties similar to those of the Milky Way nucleus. Inclusion of anomalous relaxation leads to the formation of less prominent cores than in the case of resonant relaxation alone, due to the lengthening of diffusion timescales for eccentric orbits. Steady-state capture rates of stars by the SBH are found to always be less, by as much as an order of magnitude, than capture rates in the presence of resonant relaxation alone.

1. INTRODUCTION

Paper I of this series (Merritt 2015a) described a numerical algorithm for integrating the Fokker-Planck equation for $f(E, L, t)$, the phase-space density of stars orbiting a supermassive black hole (SBH) at the center of a galaxy; E and L are respectively the orbital energy and angular momentum per unit mass of a star. Paper II (Merritt 2015b) presented steady-state and time-dependent solutions for f based on diffusion coefficients that describe the effects of both “classical” (random) and “resonant” (correlated) relaxation; the latter becomes progressively more important relative to the former as one moves inside the gravitational influence sphere of the SBH. A single value for the stellar mass, m_* , was assumed in both papers.

This paper extends the treatment of Paper II to include the qualitatively different sort of evolution experienced by eccentric orbits near a SBH (Merritt et al. 2011). Such orbits undergo rapid apsidal precession due to the effects of general relativity (GR), at an orbit-averaged rate

$$\left| \frac{d\omega}{dt} \right| = \frac{3(GM_\bullet)^{3/2}}{a^{5/2}(1-e^2)c^2} \quad (1)$$

(“Schwarzschild precession”; Merritt 2013, Equation 4.205). Here a and e are the orbital semimajor axis and eccentricity respectively and ω is the argument of periapsis. Precession described by Equation (1) affects the collective evolution in two, distinct ways. (i) The “coherence time” is defined as the mean precession time for orbits at a given energy (Rauch & Tremaine 1996). Near the SBH coherence times become progressively shorter due to Schwarzschild precession. This effect was correctly accounted for in Papers I and II and in many earlier treatments of resonant relaxation. (ii) At any energy, sufficiently eccentric orbits undergo apsidal precession on a shorter timescale than other orbits of the same energy, due to the strong eccentricity dependence of Equation (1). Such high-eccentricity orbits might be expected to evolve in a manner qualitatively different than described by the equations of resonant relaxation, since their orientation with respect to the torquing potential changes in a time short compared with the coherence time.

Since it is the high-eccentricity orbits that are most amenable to capture by the SBH, Schwarzschild precession was recognized early on as a potentially important mediating factor with regard to rates of capture from tightly-bound orbits around a SBH (Hopman & Alexander 2006b; Madigan et al. 2011).

The first, fully self-consistent investigation of orbital evolution in this regime (Merritt et al. 2011) revealed a new phenomenon. Stars near the SBH undergo random walks in angular momentum due to resonant relaxation, but when their eccentricities reach a certain maximum value (depending on a), their trajectories “bounce,” returning after roughly one coherence time to lower values of e , where they continue to evolve under the influence of resonant relaxation. The locus of reflection in the (a, e) plane was termed the “Schwarzschild barrier” (SB) and an approximate analytic expression for its location, $L = L_{\text{SB}}(E)$, was derived. Subsequent studies have confirmed this phenomenon using different integration schemes for the N -body equations of motion (Brem et al. 2014; Hamers, Portegies Zwart & Merritt 2014).

A characteristic of motion near and below the SB ($L \lesssim L_{\text{SB}}(E)$) is that the apsidal precession time is short compared with the coherence time, and with the time over which resonant relaxation would be able to change L in the absence of the rapid precession. Angular momentum evolution in the region below the SB was called “anomalous relaxation” by Hamers, Portegies Zwart & Merritt (2014). This name reflects the fact the evolution in this regime is qualitatively different than the evolution described by the equations of either classical or resonant relaxation. For instance: diffusion rates in this regime drop rapidly with decreasing L , and there is a net drift in the direction of increasing L .

The direct N -body integrations of Merritt et al. (2011) showed that the SB is not completely impermeable, although captures by the SBH were found to occur at a rate that was about an order of magnitude lower than in simulations that omitted the first post-Newtonian (1PN) terms from the equations of motion; that is, the terms that generate Schwarzschild precession. Extrapolating the capture rates in those small- N simulations to real galaxies is not straightforward. One reason is the absence, in the N -body models, of stars initially distant from the SBH that would diffuse inward and replace those lost to the SBH, thus establishing a steady state. Another reason was pointed out by Hamers et al. (2014). At sufficiently low L , anomalous diffusion rates can become so low that *classical* relaxation once again sets the timescale for angular momentum evolution. Using an approximate test-particle algorithm, Hamers et al. were able to simulate systems of much larger N and to cleanly delineate three regimes of angular momentum evolution, at energies for which the SB exists:

1. $L_{\text{SB}}(E) \lesssim L \leq 1$ (resonant relaxation)
2. $L_{\text{NR}}(E) \lesssim L \lesssim L_{\text{SB}}(E)$ (anomalous relaxation)
3. $L_{\text{lc}}(E) \leq L \lesssim L_{\text{NR}}(E)$ (classical relaxation)

(see their Figure 1). Here L_{NR} is the angular momentum at which Schwarzschild precession is so rapid that the torques driving resonant relaxation are almost completely ineffective at changing L , so that classical relaxation dominates the evolution once more. L_{lc} is the angular momentum at the edge of the loss cone. Hamers, Portegies Zwart & Merritt (2014) derived an approximate expression for $L_{\text{NR}}(E)$ and showed that in the simulations of Merritt et al. (2011), classical relaxation dominated the evolution in L over much of the (a, e) plane, including even some regions with $L > L_{\text{SB}}(E)$. They argued that this fact would complicate the extrapolation of the N -body results to real galaxies.

This paper, the third in a series, addresses these issues by incorporating into the Fokker-Planck algorithm expressions for the diffusion coefficients that account for anomalous relaxation. By integrating $f(E, L)$ forward in time using these new diffusion coefficients, steady-state solutions are constructed that are valid fully into the “Schwarzschild” regime defined in Paper II – roughly an order of magnitude nearer to the SBH than the solutions of Paper II, or indeed any other published simulation.

Section 2 reviews the numerical algorithm used here; further details are given in Papers I and II. Section 3 presents the functional forms adopted for the anomalous diffusion coefficients. Since there does not yet exist a good theory for orbital evolution in this regime, different parametrized forms for the diffusion coefficients are considered and constrained by comparison with previously-published simulations. Section 4 presents steady-state solutions for $f(E, L)$ with parameters chosen to describe the nuclear cluster of the Milky Way; the results are compared with those of Paper II that did not incorporate anomalous relaxation. Section 5 discusses some implications of the results obtained here and §6 sums up.

2. METHOD

As in Papers I and II, stars are assumed to have a single mass, m_* , and to be close enough to the black hole (SBH) that the gravitational potential defining their unperturbed orbits is

$$\Phi(r) = -\frac{GM_{\bullet}}{r} \equiv -\psi(r) \quad (2)$$

with M_{\bullet} the SBH mass, assumed constant in time. Unperturbed orbits respect the two isolating integrals E , the energy per unit mass, and L , the angular momentum per unit mass. Following Cohn & Kulsrud (1978) these are replaced by \mathcal{E} and \mathcal{R} where

$$\mathcal{E} \equiv -E = -\frac{v^2}{2} + \psi(r), \quad \mathcal{R} \equiv \frac{L^2}{L_c^2}; \quad (3)$$

$L_c(\mathcal{E})$ is the angular momentum of a circular orbit of energy \mathcal{E} so that $0 \leq \mathcal{R} \leq 1$. \mathcal{E} and \mathcal{R} are related to the semimajor axis a and eccentricity e of the Kepler orbit via

$$a = \frac{GM_{\bullet}}{2\mathcal{E}}, \quad e^2 = 1 - \mathcal{R}. \quad (4)$$

Spin of the SBH is ignored.

The time dependence of the phase-space number density of stars, $f(\mathcal{E}, \mathcal{R})$, is described by the orbit-averaged Fokker-Planck equation

$$\begin{aligned} \mathcal{J} \frac{\partial f}{\partial t} &= -\frac{\partial}{\partial \mathcal{E}} (\mathcal{J} \phi_{\mathcal{E}}) - \mathcal{J} \frac{\partial}{\partial \mathcal{R}} \phi_{\mathcal{R}}, \\ -\phi_{\mathcal{E}} &= D_{\mathcal{E}\mathcal{E}} \frac{\partial f}{\partial \mathcal{E}} + D_{\mathcal{E}\mathcal{R}} \frac{\partial f}{\partial \mathcal{R}} + D_{\mathcal{E}} f, \quad -\phi_{\mathcal{R}} = D_{\mathcal{R}\mathcal{E}} \frac{\partial f}{\partial \mathcal{E}} + D_{\mathcal{R}\mathcal{R}} \frac{\partial f}{\partial \mathcal{R}} + D_{\mathcal{R}} f \end{aligned} \quad (5)$$

with flux coefficients

$$\begin{aligned} D_{\mathcal{E}} &= -\langle \Delta \mathcal{E} \rangle - \frac{5}{4\mathcal{E}} \langle (\Delta \mathcal{E})^2 \rangle + \frac{1}{2} \frac{\partial}{\partial \mathcal{E}} \langle (\Delta \mathcal{E})^2 \rangle + \frac{1}{2} \frac{\partial}{\partial \mathcal{R}} \langle \Delta \mathcal{E} \Delta \mathcal{R} \rangle, \\ D_{\mathcal{R}} &= -\langle \Delta \mathcal{R} \rangle - \frac{5}{4\mathcal{E}} \langle \Delta \mathcal{E} \Delta \mathcal{R} \rangle + \frac{1}{2} \frac{\partial}{\partial \mathcal{E}} \langle \Delta \mathcal{E} \Delta \mathcal{R} \rangle + \frac{1}{2} \frac{\partial}{\partial \mathcal{R}} \langle (\Delta \mathcal{R})^2 \rangle, \\ D_{\mathcal{E}\mathcal{E}} &= \frac{1}{2} \langle (\Delta \mathcal{E})^2 \rangle, \quad D_{\mathcal{E}\mathcal{R}} = D_{\mathcal{R}\mathcal{E}} = \frac{1}{2} \langle \Delta \mathcal{E} \Delta \mathcal{R} \rangle, \quad D_{\mathcal{R}\mathcal{R}} = \frac{1}{2} \langle (\Delta \mathcal{R})^2 \rangle \end{aligned} \quad (6)$$

and $\mathcal{J} \equiv \sqrt{2}\pi^3 G^3 M_{\bullet}^3 \mathcal{E}^{-5/2}$ (Merritt 2013, 5.5.1). Quantities in $\langle \rangle$ are orbit-averaged diffusion coefficients. The functional forms of the diffusion coefficients are discussed below.

Loss of stars into the SBH is controlled by the choice of r_{lc} , the radius of the physical loss sphere around the SBH, and by the conditions imposed on f at the loss-cone boundary, $\mathcal{R} = \mathcal{R}_{\text{lc}}(\mathcal{E})$, defined as

$$\mathcal{R}_{\text{lc}}(\mathcal{E}) = 2 \frac{\mathcal{E}}{\mathcal{E}_{\text{lc}}} \left(1 - \frac{1}{2} \frac{\mathcal{E}}{\mathcal{E}_{\text{lc}}} \right), \quad \mathcal{E} \leq \mathcal{E}_{\text{lc}}, \quad \mathcal{E}_{\text{lc}} \equiv \frac{GM_{\bullet}}{2r_{\text{lc}}}. \quad (7)$$

\mathcal{R}_{lc} is the normalized angular momentum of an orbit with (Newtonian) periapsis at r_{lc} . The \mathcal{R} -directed flux of stars across the loss-cone boundary is

$$F(\mathcal{E}) d\mathcal{E} = -\mathcal{J}(\mathcal{E}) \phi_{\mathcal{R}}(\mathcal{R}_{\text{lc}}) d\mathcal{E} \equiv -\mathcal{J}(\mathcal{E}) \phi_{\mathcal{R},\text{lc}}(\mathcal{E}) d\mathcal{E}. \quad (8)$$

Two quantities that play important roles in angular momentum diffusion near the loss-cone boundary are \mathcal{D} ,

$$\mathcal{D}(\mathcal{E}) \equiv \frac{\langle (\Delta \mathcal{R})^2 \rangle_t}{2\mathcal{R}} \Big|_{\mathcal{R}=\mathcal{R}_{\text{lc}}} = \frac{D_{\mathcal{R}\mathcal{R}}(\mathcal{E}, \mathcal{R}_{\text{lc}})}{\mathcal{R}_{\text{lc}}} \quad (9)$$

and q_{lc} ,

$$q_{\text{lc}}(\mathcal{E}) \equiv \frac{P(\mathcal{E})\mathcal{D}(\mathcal{E})}{\mathcal{R}_{\text{lc}}(\mathcal{E})}. \quad (10)$$

\mathcal{D}^{-1} is effectively an orbit-averaged, angular momentum relaxation time at energy \mathcal{E} . The quantity q_{lc} measures the change in angular momentum per orbital period, compared with the size of the loss cone. The loss-cone boundary conditions adopted in all the integrations presented here were the ‘‘Cohn-Kulsrud boundary conditions’’ defined in Paper I. No attempt is made to solve for f inside the loss cone, i.e. at $\mathcal{R} < \mathcal{R}_{\text{lc}}$, since f does not satisfy Jeans’s theorem in this region.

Solutions are obtained on a $(N_x \times N_z)$ grid in (X, Z) , where

$$\begin{aligned} X &\equiv \ln R = \ln \left[\frac{L}{L_c(\mathcal{E})} \right]^2, \\ Z &\equiv \ln(1 + \beta \mathcal{E}^*) = \ln(1 + \beta \mathcal{E}/c^2). \end{aligned} \quad (11)$$

Integrations presented here used $N_x = N_z = 64$ grid points. The code adopts units such that

$$G = M_{\bullet} = c = 1 \quad (12)$$

allowing the results to be scaled to different masses of the SBH. Dimensionless parameters that must be specified before the start of an integration include m_{\star}/M_{\bullet} , $\ln \Lambda$ and $\Theta_{\text{lc}} \equiv r_{\text{lc}}/r_g$.

In Paper II, the diffusion coefficients had the forms

$$\begin{aligned} \langle \Delta \mathcal{E} \rangle &= \langle \Delta \mathcal{E} \rangle_{\text{CK}}, \quad \langle (\Delta \mathcal{E})^2 \rangle = \langle (\Delta \mathcal{E})^2 \rangle_{\text{CK}}, \quad \langle \Delta \mathcal{E} \Delta \mathcal{R} \rangle = \langle \Delta \mathcal{E} \Delta \mathcal{R} \rangle_{\text{CK}}, \\ \langle \Delta \mathcal{R} \rangle &= \langle \Delta \mathcal{R} \rangle_{\text{CK}} + \langle \Delta \mathcal{R} \rangle_{\text{RR}}, \quad \langle (\Delta \mathcal{R})^2 \rangle = \langle (\Delta \mathcal{R})^2 \rangle_{\text{CK}} + \langle (\Delta \mathcal{R})^2 \rangle_{\text{RR}}. \end{aligned} \quad (13)$$

The subscript CK indicates that the diffusion coefficient is computed as in Cohn & Kulsrud (1978); their derivation was based on standard assumptions about randomness of encounters (Rosenbluth et al. 1957). The subscript RR refers to ‘‘resonant relaxation’’ (Rauch & Tremaine 1996). The resonant diffusion coefficients were expressed as

$$\langle \Delta \mathcal{R} \rangle_{\text{RR}} = 2A(\mathcal{E})(1 - 2\mathcal{R}), \quad \langle (\Delta \mathcal{R})^2 \rangle_{\text{RR}} = 4A(\mathcal{E})\mathcal{R}(1 - \mathcal{R}). \quad (14)$$

The term containing the \mathcal{E} dependence is

$$A(a) = \alpha_s^2 \left[\frac{M_\bullet}{M_\star} \right]^2 \frac{1}{N} \frac{t_{\text{coh}}}{P^2}, \quad \alpha_s = 1.6, \quad a = \frac{GM_\bullet}{2\mathcal{E}}. \quad (15)$$

Here $N \equiv N(r < a)$ is the number of stars instantaneously at radii than a , $M_\star = m_\star N$, P is the Kepler (radial) period, and t_{coh} is the coherence time, defined as

$$t_{\text{coh}}^{-1} \equiv t_{\text{coh,M}}^{-1} + t_{\text{coh,S}}^{-1},$$

$$t_{\text{coh,M}}(a) = \frac{M_\bullet}{Nm_\star} P, \quad t_{\text{coh,S}}(a) = \frac{1}{12} \frac{a}{r_g} P. \quad (16)$$

$t_{\text{coh,M}}$ is the mean precession time for stars of semimajor axis a due to the distributed mass around the SBH (“mass precession”), and $t_{\text{coh,S}}$ is the mean precession time due to the 1PN corrections to the Newtonian equations of motion (“Schwarzschild precession”).

3. ANOMALOUS DIFFUSION COEFFICIENTS

The diffusion coefficients (13) are affected by general relativity (GR) to the extent that GR determines the coherence time via equation (16). Another GR-related phenomenon is the Schwarzschild barrier (SB), the tendency of orbits near the SBH to avoid high eccentricities. The SB was first observed in N -body simulations (Merritt et al. 2011), as a locus in the (E, L) plane where trajectories “bounced” during the course of their random walks in L . At energies where the angular momentum associated with the bounce, $L_{\text{SB}}(E)$, exceeds $L_{\text{lc}}(E)$, far fewer stars are captured by the SBH than in simulations that neglect the effects of GR. The Merritt et al. (2011) study revealed that orbits experiencing the “bounce” were of such high eccentricity that their GR precession times were short compared with those of typical (i.e., less eccentric) stars at the same a .

Hamers, Portegies Zwart & Merritt (2014) coined the term “anomalous relaxation” to describe the behavior of orbits in this high-eccentricity regime, $L \lesssim L_{\text{SB}}(E)$. Those authors verified the existence of the SB via an independent set of N -body integrations, and also carried out test-particle integrations, using a much larger number of stars, from which they numerically evaluated the rates of diffusion in the anomalous regime.

Based on these, and other, studies, two analytic expressions have been proposed for the location of the SB. The first compares the GR precession time with the time for the \sqrt{N} torques to change L (Merritt et al. 2011):

$$\mathcal{R}_{\text{SB}}^{(i)}(a) \approx \left(\frac{r_g}{a} \right)^2 \left[\frac{M_\bullet}{M_\star(a)} \right]^2 N(a). \quad (17)$$

The second (Hamers, Portegies Zwart & Merritt 2014; Bar-Or & Alexander 2014) compares the GR precession time with the coherence time:

$$\mathcal{R}_{\text{SB}}^{(ii)}(a) \approx 4 \frac{r_g}{a} \frac{t_{\text{coh}}(a)}{P(a)}. \quad (18)$$

In spite of their disparate functional forms, the two expressions can yield numerically similar relations for $\mathcal{R}_{\text{SB}}(a)$, as illustrated below. The former relation appears to more accurately reproduce the barrier location in numerical studies to date; while the latter relation arises naturally when matching diffusion coefficients in the resonant and anomalous regimes (Hamers, Portegies Zwart & Merritt 2014).

Evaluating the former expression in the case of an unmodified Bahcall-Wolf cusp, $n(r) \propto r^{-7/4}$, yields

$$\frac{a_{\text{SB}}}{r_g} \approx \left(\frac{M_\bullet}{2m_\star} \right)^{4/13} \left(\frac{r_m}{r_g} \right)^{5/13} (1 - e^2)^{-4/13} \quad (19)$$

where r_m is the radius containing a mass in stars of $2M_\bullet$. The barrier as given by Equation (19) extends between the radii a_{min} and a_{max} , where

$$\frac{a_{\text{min}}}{r_g} \approx \left(\frac{M_\bullet}{2m_\star} \right)^{4/13} \left(\frac{r_m}{r_g} \right)^{5/13}, \quad (20a)$$

$$\frac{a_{\text{max}}}{r_g} \approx (4\Theta)^{-4/9} \left(\frac{M_\bullet}{m_\star} \right)^{4/9} \left(\frac{r_m}{r_g} \right)^{5/9}. \quad (20b)$$

The first relation follows from setting $e = 0$. The second relation is the intersection of Equation (19) with the curve $a(1 - e) = \Theta r_g$, the periapsis of an orbit that intersects the loss sphere of radius $r_{\text{lc}} = \Theta r_g$. Taking parameter values appropriate for the Milky Way:

$$M_\bullet = 4 \times 10^6 M_\odot, \quad m_\star = 1, \quad \Theta = 15$$

yields

$$a_{\min} \approx 6 \left(\frac{r_m}{\text{pc}} \right)^{5/13} \text{ mpc}, \quad a_{\max} \approx 140 \left(\frac{r_m}{\text{pc}} \right)^{5/9} \text{ mpc}. \quad (21)$$

“Anomalous relaxation” is defined as angular-momentum diffusion of orbits with $L \lesssim L_{\text{SB}}(E)$. Paper I presented a derivation, based on a simple Hamiltonian model, of the diffusion coefficients in the anomalous regime:

$$\langle \Delta \mathcal{R} \rangle_{\text{AR}} = \frac{5}{\tau} \mathcal{R}^2, \quad \langle (\Delta \mathcal{R})^2 \rangle_{\text{AR}} = \frac{4}{\tau} \mathcal{R}^3 \quad (22)$$

where $\tau(a) \equiv t_{\text{coh}}(a)/(A_{\sqrt{N}})^2$ and

$$A_{\sqrt{N}} \equiv \frac{1}{2\sqrt{N(a)}} \frac{M_*(a)}{M_\bullet} \frac{a}{r_g}. \quad (23)$$

The rapid, power-law drop predicted in the diffusion rates for $\mathcal{R} < \mathcal{R}_{\text{SB}}$ is due to the adiabatic invariance of L under the effects of rapid precession.

The derivation leading to equations (22)-(23) was very approximate and one would like to verify those functional forms by comparison with N -body integrations. Hamers, Portegies Zwart & Merritt (2014) attempted to do this. However, it was found that the value of N accessible to high-accuracy simulations ($N \lesssim 100$) was so small that the effects of anomalous relaxation could not be cleanly differentiated from the effects of classical relaxation at small L . Application of a more approximate, test-particle approach allowed Hamers et al. to increase the effective value of N by two orders of magnitude. The diffusion coefficients extracted from these experiments were found to be reasonably well described by equations (22)-(23).

In the present treatment, we account for the effects of anomalous relaxation by modifying the angular momentum diffusion coefficients (13). We consider two sorts of modification with different functional forms: a power-law modification, which reproduces equations (22) at small \mathcal{R} ; and an exponential modification, which implies a much more rapid decrease in the diffusion rate toward small \mathcal{R} .

3.1. Power-law modification

To account for anomalous relaxation, the angular-momentum diffusion coefficients of Equation (13) are modified as follows:

$$\langle \Delta \mathcal{R} \rangle = \langle \Delta \mathcal{R} \rangle_{\text{CK}} + g_1(\mathcal{E}, \mathcal{R}) \langle \Delta \mathcal{R} \rangle_{\text{RR}}, \quad \langle (\Delta \mathcal{R})^2 \rangle = \langle (\Delta \mathcal{R})^2 \rangle_{\text{CK}} + g_2(\mathcal{E}, \mathcal{R}) \langle (\Delta \mathcal{R})^2 \rangle_{\text{RR}}. \quad (24)$$

The functions $g_1(\mathcal{R})$ and $g_2(\mathcal{R})$ should have certain properties. Both g_1 and g_2 should tend to one as $\mathcal{R} \rightarrow 1$. **Since**

$$\langle \Delta \mathcal{R} \rangle_{\text{RR}} \rightarrow 2A(\mathcal{E}), \quad \langle (\Delta \mathcal{R})^2 \rangle_{\text{RR}} \rightarrow 4A(\mathcal{E})\mathcal{R}$$

as $\mathcal{R} \rightarrow 0$ (Equation 14), we require $g_1 \rightarrow \mathcal{R}^2$ and $g_2 \rightarrow \mathcal{R}^2$ for small \mathcal{R} so that the small- \mathcal{R} behavior of Equation (22) is reproduced. The transition between the two regimes should occur at $\mathcal{R} \sim \mathcal{R}_{\text{SB}}$ for both functions.

An ad hoc functional form for g_2 that satisfies these requirements is

$$g_2(\mathcal{E}, \mathcal{R}) = \left\{ 1 + \left[\frac{R_2(\mathcal{E})}{\mathcal{R}} \right]^n \right\}^{-2/n} \quad (25)$$

where $\mathcal{R}_2 \approx \mathcal{R}_{\text{SB}}(\mathcal{E})$. The parameter n determines the rapidity of transition between the large- \mathcal{R} and small- \mathcal{R} regimes.

The same functional form might be adopted for g_1 . Rather than make that choice, we first consider another possible constraint on g_1 and g_2 .

The \mathcal{R} -directed flux coefficients that appear in the Fokker-Planck equation are given by Equations (6):

$$D_{\mathcal{R}} = -\langle \Delta \mathcal{R} \rangle - \frac{5}{4\mathcal{E}} \langle \Delta \mathcal{E} \Delta \mathcal{R} \rangle + \frac{1}{2} \frac{\partial}{\partial \mathcal{E}} \langle \Delta \mathcal{E} \Delta \mathcal{R} \rangle + \frac{1}{2} \frac{\partial}{\partial \mathcal{R}} \langle (\Delta \mathcal{R})^2 \rangle \quad (26a)$$

$$\approx -\langle \Delta \mathcal{R} \rangle + \frac{1}{2} \frac{\partial}{\partial \mathcal{R}} \langle (\Delta \mathcal{R})^2 \rangle, \quad (26b)$$

$$D_{\mathcal{R}\mathcal{R}} = \frac{1}{2} \langle (\Delta \mathcal{R})^2 \rangle. \quad (26c)$$

Since the \mathcal{R} -directed flux is

$$\phi_{\mathcal{R}} = -D_{\mathcal{R}\mathcal{E}} \frac{\partial f}{\partial \mathcal{E}} - D_{\mathcal{R}\mathcal{R}} \frac{\partial f}{\partial \mathcal{R}} - D_{\mathcal{R}} f \approx -D_{\mathcal{R}\mathcal{R}} \frac{\partial f}{\partial \mathcal{R}} - D_{\mathcal{R}} f, \quad (27)$$

it is reasonable to require that the diffusion coefficients in \mathcal{R} satisfy

$$D_{\mathcal{R}} \rightarrow 0, \quad D_{\mathcal{R}\mathcal{R}} \rightarrow 0 \quad (28)$$

at the boundaries $\mathcal{R} = \{0, 1\}$; in other words, that

$$\langle \Delta \mathcal{R} \rangle = \frac{1}{2} \frac{\partial}{\partial \mathcal{R}} \langle (\Delta \mathcal{R})^2 \rangle, \quad \langle (\Delta \mathcal{R})^2 \rangle = 0 \quad (29a)$$

at $\mathcal{R} = \{0, 1\}$. Both the classical (Cohn-Kulsrud), and the resonant diffusion coefficients adopted here and in Papers I and II satisfy these conditions.

Suppose that a stronger condition is imposed: $D_{\mathcal{R}} \equiv 0$, $0 \leq \mathcal{R} \leq 1$. In this case, the Fokker-Planck equation describing diffusion in angular momentum reduces to

$$\frac{\partial f}{\partial t} = -\frac{\partial \phi_{\mathcal{R}}}{\partial \mathcal{R}} = \frac{\partial}{\partial \mathcal{R}} \left(D_{\mathcal{R}} \frac{\partial f}{\partial \mathcal{R}} \right) = \frac{1}{2} \frac{\partial}{\partial \mathcal{R}} \left(\langle (\Delta \mathcal{R})^2 \rangle \frac{\partial f}{\partial \mathcal{R}} \right) \quad (30)$$

which has a steady-state (zero-flux) solution $f(\mathcal{R}) = \text{constant}$ regardless of the functional form of $\langle (\Delta \mathcal{R})^2 \rangle$. It could be argued that $f(\mathcal{R}) = \text{constant}$ is a reasonable form for a time-independent f , since it corresponds to an isotropic, or “maximum entropy,” state. The resonant diffusion coefficients adopted in Papers I and II satisfy this stronger condition. Setting $D_{\mathcal{R}} \equiv 0$ also implies zero drift, i.e., zero flux in \mathcal{R} in the absence of a gradient. For this reason, $D_{\mathcal{R}} \equiv 0$ will henceforth be called a “zero-drift” condition.

Returning now to the anomalous diffusion coefficients, we ask: what functional form for g_1 is required for zero drift? That is:

$$0 = D_{\mathcal{R}} = -g_1(\mathcal{R}) \langle \Delta \mathcal{R} \rangle_{\text{RR}} + \frac{1}{2} \frac{\partial}{\partial \mathcal{R}} [g_2(\mathcal{R}) \langle (\Delta \mathcal{R})^2 \rangle_{\text{RR}}]. \quad (31)$$

Assuming that g_2 is given by Equation (25), the result is

$$g_1(\mathcal{R}) = \left\{ 1 + \left[\frac{R_2(\mathcal{E})}{\mathcal{R}} \right]^n \right\}^{-2/n} + \frac{2(1-\mathcal{R})}{1-2\mathcal{R}} \left(\frac{\mathcal{R}_2}{\mathcal{R}} \right)^n \left\{ 1 + \left[\frac{R_2(\mathcal{E})}{\mathcal{R}} \right]^n \right\}^{-2/n-1}. \quad (32)$$

Since the zero-drift argument is one of plausibility only, we will consider a slightly more general expression for g_1 that includes “zero drift” as a special case:

$$g_1(\mathcal{R}) = \left\{ 1 + \left[\frac{R_1(\mathcal{E})}{\mathcal{R}} \right]^n \right\}^{-2/n} + \frac{2(1-\mathcal{R})}{1-2\mathcal{R}} \left(\frac{\mathcal{R}_1}{\mathcal{R}} \right)^n \left\{ 1 + \left[\frac{R_1(\mathcal{E})}{\mathcal{R}} \right]^n \right\}^{-2/n-1}. \quad (33)$$

The only difference between Equations (32) and (33) is the introduction of a second parameter, \mathcal{R}_1 , in place of \mathcal{R}_2 . This generalization still satisfies the zero-flux condition (28) at $\mathcal{R} = 0$, regardless of $\mathcal{R}_1/\mathcal{R}_2$. At $\mathcal{R} = 1$, g_1 and g_2 are both very close to one (especially since n will be chosen to be large) so that the resonant diffusion coefficients are recovered and the zero-flux condition is satisfied, again for any choice of $\mathcal{R}_1/\mathcal{R}_2$.

Correspondence of these expressions with the diffusion coefficients of Equation (22) at small \mathcal{R} would require

$$\mathcal{R}_1^2(\mathcal{E}) = (6/5)\tau A(\mathcal{E}), \quad \mathcal{R}_2^2(\mathcal{E}) = \tau A(\mathcal{E}), \quad (34)$$

where

$$\tau A(\mathcal{E}) = 4\alpha_s^2 \left(\frac{t_{\text{coh}}}{P} \right)^2 \left(\frac{r_g}{a} \right)^2. \quad (35)$$

To within factors of order unity, these relations imply $\mathcal{R}_1 \approx \mathcal{R}_2 \approx \mathcal{R}_{\text{SB}}^{(ii)}$ (equation 18).

It is shown in the Appendix that at small \mathcal{R} , these choices for g_1 and g_2 imply

$$D_{\mathcal{R}} \rightarrow 6\lambda A(\mathcal{E}) \left(\frac{\mathcal{R}}{\mathcal{R}_2} \right)^2, \quad \lambda \equiv 1 - \frac{\mathcal{R}_2^2}{\mathcal{R}_1^2} \quad (36)$$

so that the direction of the drift is determined by the relative sizes of \mathcal{R}_1 and \mathcal{R}_2 , as follows:

$$\mathcal{R}_1 < \mathcal{R}_2 \rightarrow D_{\mathcal{R}} < 0 \rightarrow \phi_{\mathcal{R}} > 0 \quad (37a)$$

$$\mathcal{R}_1 > \mathcal{R}_2 \rightarrow D_{\mathcal{R}} > 0 \rightarrow \phi_{\mathcal{R}} < 0 \quad (37b)$$

where the expressions for $\phi_{\mathcal{R}}$ assume $f(\mathcal{R}) = \text{constant}$. Furthermore both the form of the steady-state $f(\mathcal{R})$, and the steady-state flux (assuming the presence of a sink, i.e. that $f(\mathcal{R}) = 0$ at $\mathcal{R} \leq \mathcal{R}_0$), depend sensitively on λ , as shown in Figures 10 and 11 from the Appendix. In the zero-drift ($\lambda = 0$) case, the steady-state flux is reduced by a factor

$$\eta \approx 2 \left(\frac{\mathcal{R}_0}{\mathcal{R}_2} \right)^2 \log \left(\frac{\mathcal{R}_2}{\mathcal{R}_0} \right) \quad (38)$$

compared with the flux that would obtain in the absence of anomalous relaxation (note that an empty loss cone has been assumed). For nonzero λ , the reduction factor can be greater or smaller than this, tending toward a maximum value of one for large $\mathcal{R}_1/\mathcal{R}_2$ (Figure 11).

3.2. Exponential modification

Bar-Or & Alexander (2014) suggested a different functional form for $\langle(\Delta\mathcal{R})^2\rangle$ in the anomalous regime:

$$\langle(\Delta\mathcal{R})^2\rangle \propto \exp\left(-\frac{1}{\pi} \frac{\mathcal{R}_{\text{SB}}^2}{\mathcal{R}^2}\right), \quad (39)$$

an exponential cut-off toward small \mathcal{R} . While there does not seem to be strong support for this functional form in any published numerical simulations, we consider it here for completeness, and because it serves to illustrate how sensitively the evolution of f depends on the form assumed for the anomalous diffusion coefficients.

Proceeding as above, we write

$$\langle\Delta\mathcal{R}\rangle = \langle\Delta\mathcal{R}\rangle_{\text{CK}} + h_1(\mathcal{E}, \mathcal{R})\langle\Delta\mathcal{R}\rangle_{\text{RR}}, \quad \langle(\Delta\mathcal{R})^2\rangle = \langle(\Delta\mathcal{R})^2\rangle_{\text{CK}} + h_2(\mathcal{E}, \mathcal{R})\langle(\Delta\mathcal{R})^2\rangle_{\text{RR}}. \quad (40)$$

Suppose

$$h_2(\mathcal{E}, \mathcal{R}) = \exp\left(-\frac{\mathcal{R}_4^2}{\mathcal{R}^2}\right) \quad (41)$$

where $\mathcal{R}_4(\mathcal{E}) \approx \mathcal{R}_{\text{SB}}(\mathcal{E})$. Since $\mathcal{R}_4 \ll 1$, $h_2(\mathcal{E}, 1) \approx 1$. The zero-drift condition would imply

$$\langle\Delta\mathcal{R}\rangle = 2A(\mathcal{E}) \left[1 - 2\mathcal{R} + 2(1 - \mathcal{R}) \left(\frac{\mathcal{R}_4}{\mathcal{R}}\right)^2\right] \exp\left(-\frac{\mathcal{R}_4^2}{\mathcal{R}^2}\right).$$

We again generalize this expression by defining a second parameter, \mathcal{R}_3 , and writing

$$h_1(\mathcal{R}) = \left[1 + \frac{2(1 - \mathcal{R})}{1 - 2\mathcal{R}} \left(\frac{\mathcal{R}_3}{\mathcal{R}}\right)^2\right] \exp\left(-\frac{\mathcal{R}_3^2}{\mathcal{R}^2}\right). \quad (42)$$

At small \mathcal{R} , these expressions imply a flux coefficient

$$D_{\mathcal{R}} \rightarrow 4A(\mathcal{E}) \left(\frac{\mathcal{R}_4}{\mathcal{R}}\right)^2 \exp\left(-\frac{\mathcal{R}_4^2}{\mathcal{R}^2}\right) \left[1 - \frac{\mathcal{R}_3^2}{\mathcal{R}_4^2} \exp\left(-\frac{\mathcal{R}_3^2 - \mathcal{R}_4^2}{\mathcal{R}^2}\right)\right] \quad (43)$$

showing that in this case, as in the power-law case, the sign of $D_{\mathcal{R}}$ is determined by the relative sizes of \mathcal{R}_3 and \mathcal{R}_4 . Figures 10 and 11 illustrate the properties of the steady-state solutions $f(\mathcal{R})$. The behavior of f at small \mathcal{R} depends very sensitively on $\mathcal{R}_3/\mathcal{R}_4$. The reduction in the steady-state flux, for $\mathcal{R}_3 = \mathcal{R}_4$, is

$$\eta \approx 2 \frac{\mathcal{R}_4}{\mathcal{R}_0} \log\left(\frac{\mathcal{R}_4}{\mathcal{R}_0}\right) e^{-\mathcal{R}_4/\mathcal{R}_0}. \quad (44)$$

3.3. Constraining the functional forms of the diffusion coefficients in the anomalous regime

Based on the analysis presented above and in the Appendix, many properties of the steady-state solutions are expected to depend sensitively on the functional forms of the diffusion coefficients in the anomalous regime, and in particular on the ratios $\mathcal{R}_1/\mathcal{R}_2$ or $\mathcal{R}_3/\mathcal{R}_4$.

In Paper I, the functional forms of the diffusion coefficients in the *resonant* regime were successfully constrained by comparison with the numerical results of Hamers, Portegies Zwart & Merritt (2014). Those authors used a test-particle integrator to extract values of the angular momentum diffusion coefficients for stars orbiting near a SBH in nuclei with $n(r) \propto r^{-2}$ and r^{-1} .

The Hamers et al. integrations included post-Newtonian terms in the equations of motion, both for the field and test stars, and the suppression of angular momentum diffusion below the Schwarzschild barrier was clearly seen. Figure 1 provides an illustration: it shows the first- and second-order diffusion coefficients for stars in a single energy bin, in integrations of a model with $n(r) \propto r^{-2}$.¹ Overplotted are analytic diffusion coefficients from the two families considered above: power-law (Equations A1, A2) and exponential (Equations A1, A23).

These figures, and similar ones made for stars at other energies, motivate the following conclusions (some of which were presented already by Hamers et al.):

1. An exponential dependence of the diffusion coefficients on \mathcal{R} in the anomalous regime (Bar-Or & Alexander 2014) is ruled out.
2. The power-law dependence of $\langle\Delta\mathcal{R}\rangle$ and $\langle(\Delta\mathcal{R})^2\rangle$ on \mathcal{R} predicted in Paper I, and reproduced here in Equations (22), is confirmed, particularly in the case of the second-order coefficient for which the noise is smallest.
3. The value of \mathcal{R} that defines the transition between the resonant and anomalous regimes, called here \mathcal{R}_2 , is well predicted by Equation (18).

¹ These data were kindly provided by A. Hamers.

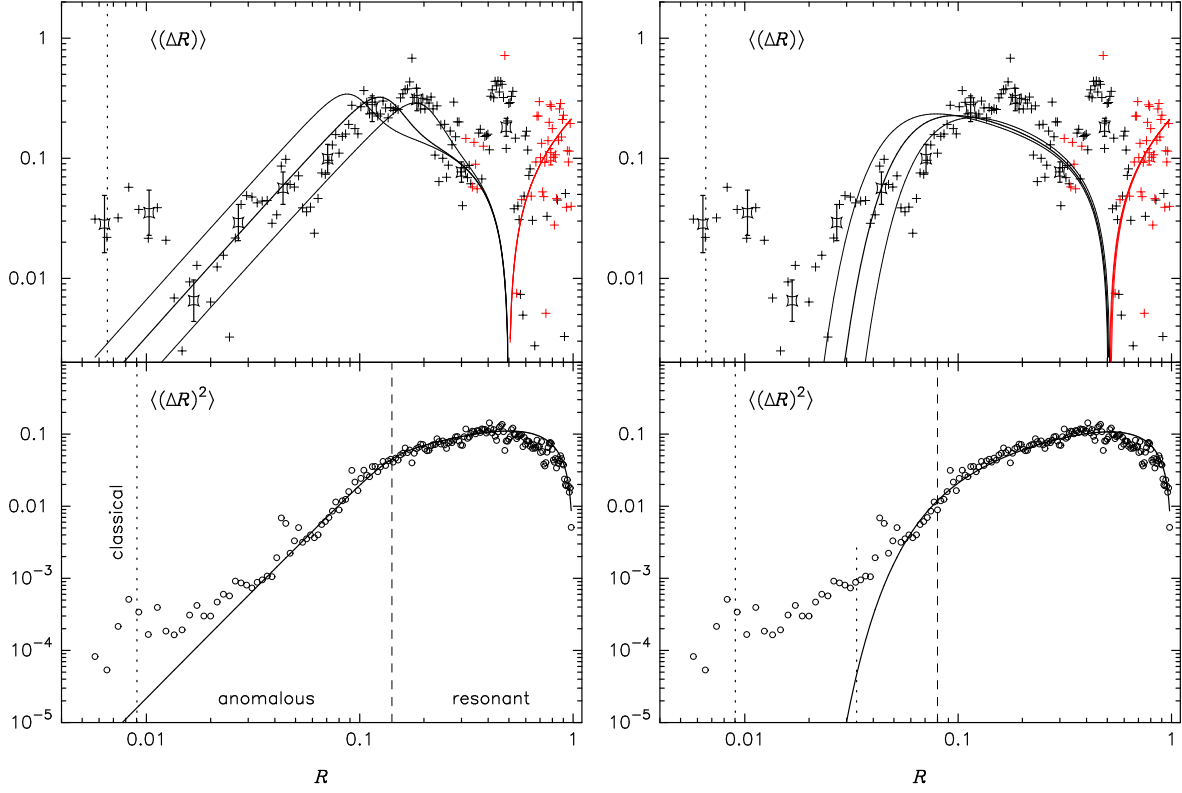


FIG. 1.— Fits to diffusion coefficients extracted from the test-particle integrations of Hamers, Portegies Zwart & Merritt (2014), for the radial bin $\langle a \rangle = 11.9$ mpc. In the upper panels, red symbols are $-\langle\Delta R\rangle$. **Diamond symbols are binned data, with errors, to guide the eye; fits were based on the unbinned data.** **Left:** analytic curves are Equations (A1), (A2), the power-law model for anomalous relaxation. $\mathcal{R}_2 = 0.110$ (shown by the dashed line in the bottom panel); in the upper panel, $\mathcal{R}_1/\mathcal{R}_2 = \{1, 1.5, 0.7\}$. **Right:** fits of the exponential model for anomalous relaxation, Equations (A1), (A23). $\mathcal{R}_4 = 0.080$, $\mathcal{R}_3/\mathcal{R}_4 = \{1, 1.25, 0.8\}$. Vertical dotted lines are estimates of the value of \mathcal{R} at which classical relaxation dominates anomalous relaxation (Eqs. 51), assuming that the power-law forms of the anomalous diffusion coefficients are correct; the analytic forms would not be expected to describe the data below these lines. In the lower-right panel, the additional dotted line at $\mathcal{R} \approx 0.33$ is Eq. (53), an estimate of where classical relaxation would begin to dominate if the exponential forms of the anomalous diffusion coefficients were correct.

An attempt was made to find the best-fit value(s) of $\mathcal{R}_1/\mathcal{R}_2$ by searching for parameter values that optimized the fits to data like those in Figure 1. Unfortunately, the results so obtained were found not to be robust. This was due in part to the greater noise associated with data below the Schwarzschild barrier, particularly in the case of the first-order coefficient. In addition, the much greater variation in the amplitudes of $\langle\Delta R\rangle$ and $\langle\langle\Delta R^2\rangle\rangle$ at a single energy meant that the best-fit solution depended sensitively on the relative weighting of the data at different values of \mathcal{R} . In the end, all that could be concluded was that the first-order diffusion coefficients are consistent with $\mathcal{R}_1 = \mathcal{R}_2$, the “zero-drift” condition; but that values of $\mathcal{R}_1/\mathcal{R}_2$ moderately greater or less than one could not be excluded using these data.

The fact that the steady-state form of $f(\mathcal{R})$, and the loss-cone flux, depend sensitively on $\mathcal{R}_1/\mathcal{R}_2$ suggests a second way to constrain the anomalous diffusion coefficients: insert them into the Fokker-Planck equation and integrate forward from initial conditions like the ones used by Merritt et al. (2011) in their small- N simulations. As discussed in Hamers et al., the value of N in those simulations was too small to allow direct extraction of the diffusion coefficients. However, the time-averaged, or integrated, properties of the N -body models were reasonably well determined, particularly given that multiple (~ 8) realizations of the same initial conditions were integrated, allowing the variance in the results to be reduced by averaging.

The Merritt et al. (2011) initial conditions consisted of 50 stars, of mass $m_\star = 50M_\odot$, distributed as $n(r) \propto r^{-2}$ around a SBH of mass $M_\bullet = 10^6 M_\odot$. The initial distribution was truncated for orbits with semi-major axes above 10 mpc and below 0.1 mpc. Integrations were carried out both with, and without, post-Newtonian terms in the equations of motion, up to order 2.5 PN. Capture of stars by the SBH was allowed to occur whenever the orbital periaapsis fell below $8r_g = 8GM_\bullet/c^2$. Each realization of the initial conditions was integrated for a time corresponding to 2×10^6 yr (with PN terms) and 10^7 yr (without PN terms). The average capture rate in the relativistic integrations was about one event per 10^6 yr; in the absence of the PN terms, mean capture rates were about a factor 20 higher.

There is no ambiguity in representing the Merritt et al. N -body initial conditions as a smooth $f(\mathcal{E}, \mathcal{R})$. However, the Fokker-Planck algorithm has a number of parameters that must be specified, in addition to those that define the anomalous diffusion coefficients (n and $\mathcal{R}_1/\mathcal{R}_2$, or $\mathcal{R}_3/\mathcal{R}_4$). Those parameters include

$$\mathcal{E}_{\min}, \quad \ln \Lambda, \quad \frac{r_{\text{lc}}}{r_g}, \quad \Delta t, \quad N_X, \quad N_Z. \quad (45)$$

\mathcal{E}_{\min} is the binding energy at the edge of the $(\mathcal{E}, \mathcal{R})$ grid; it should be small enough that few stars diffuse to $\mathcal{E} < \mathcal{E}_{\min}$ during the course of the integration. The value $10^{-8}c^2$ was chosen, which is the energy of an orbit with semimajor axis $a = 5 \times 10^7 r_g \approx 2.5$ pc, or ~ 250 times the maximum a -value of the initial conditions. The number of grid points was $N_X = N_Z = 64$. The quantity $\ln \Lambda$ was set to 15 in most of the integrations, except for one set in which smaller and larger values (from 11 to 19) were tried. The Coulomb logarithm only appears in the expressions for the classical diffusion coefficients; since evolution of these models is dominated by resonant relaxation, the results are expected to be weakly dependent on $\ln \Lambda$ and this was found to be the case. The integration time step, Δt , was set to 2000 yr, i.e. 10^3 steps per integration.

A natural choice for the parameter r_{1c}/r_g in the Fokker-Planck integrations would be 8, the same value assumed in the N -body integrations. In the case of “plunges” – captures that occur without significant energy loss due to gravitational radiation – this would be the correct choice. However, some of the N -body capture events were “EMRIs,” for which capture was preceded by significant energy loss due to the 2.5PN terms. No such loss terms are included in the Fokker-Planck integrations described here. Roughly speaking, the effect of the 2.5PN terms is to shift the location of the loss cone toward larger \mathcal{R} (i.e. larger orbital periastris) at each \mathcal{E} (see e.g. Figure 5 of Merritt et al. 2011). To evaluate the effect on the Fokker-Planck results of ignoring the 2.5PN terms, a set of integrations was carried out setting $r_{1c}/r_g = 32$, four times its value in the N -body integrations.

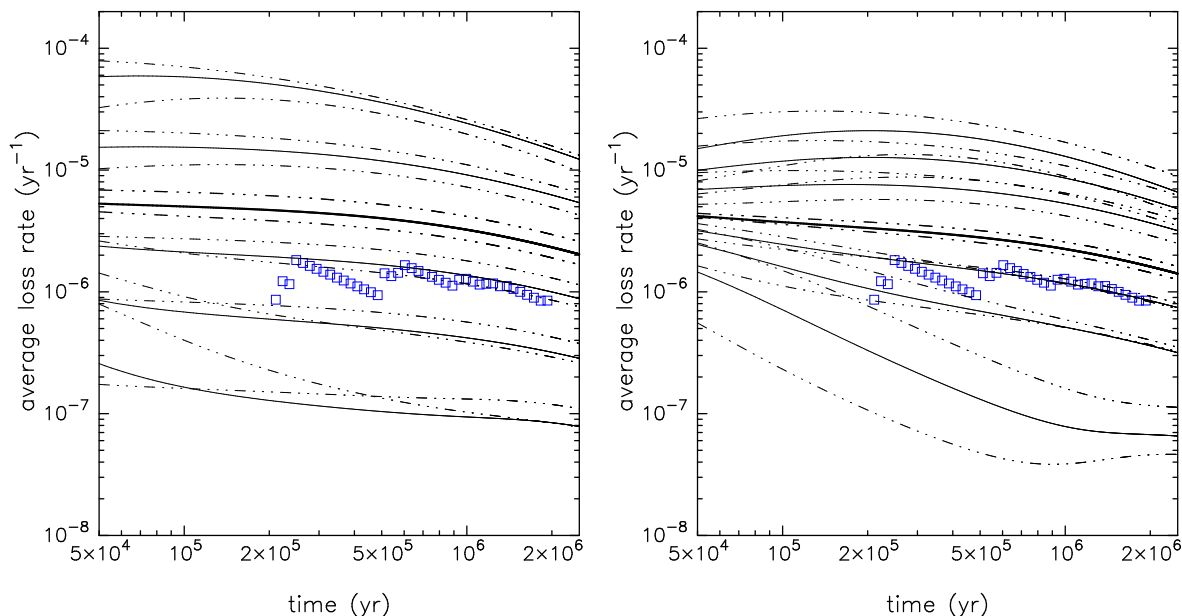


FIG. 2.— Time-averaged loss rates, defined as the total number of stars lost until time t , divided by t . (Blue) squares are from the N -body integrations of Merritt et al. (2011) (Figure 2c of that paper); curves are from the Fokker-Planck integrations described in §3.3. **The sudden jumps in the N -body loss rates at early times correspond to single capture events.** Left (right) panel shows results using the power-law (exponential) forms of the anomalous diffusion coefficients in the Fokker-Planck code. **Left:** the six sets of curves are for $\mathcal{R}_1/\mathcal{R}_2 = \{2, 1.2, 1, 0.9, 0.8, 0.7\}$, from top to bottom. The different line styles are explained in the text. **Right:** the six sets of curves are for $\mathcal{R}_3/\mathcal{R}_4 = \{1.4, 1.2, 1.1, 1, 0.95, 0.9, 0.7\}$, from top to bottom. Curves for $\mathcal{R}_1/\mathcal{R}_2 = 1$ or $\mathcal{R}_3/\mathcal{R}_4 = 1$ (“zero drift”) are thicker.

Figure 2 compares time-averaged loss rates in the N -body and Fokker-Planck models, defined as the total number of stars lost until time t divided by t . The left panel shows results using the power-law forms of the anomalous diffusion coefficients, Equations (A1), (A2), with $n = 8$; the right panel shows results using the exponential forms, Equations (A1), (A23). Each panel shows results for several values of $\mathcal{R}_1/\mathcal{R}_2$ (power-law) or $\mathcal{R}_3/\mathcal{R}_4$ (exponential), as specified in the caption. For each value of this ratio, three integrations were carried out, varying the way in which \mathcal{R}_2 or \mathcal{R}_4 were related to \mathcal{R}_{SB} . One of the three integrations (shown by the solid curves) equated \mathcal{R}_2 or \mathcal{R}_4 with $\mathcal{R}_{\text{SB}}^{(ii)}$, Equation (18). The other two integrations adopted larger or smaller values: by a factor two or one-half (in the power-law models), or by a factor $\sqrt{\pi}$ or $1/\sqrt{\pi}$ (exponential). These additional integrations are shown by the dash-dotted curves in Figure 2. Larger (smaller) values of \mathcal{R}_2 or \mathcal{R}_4 generally resulted in smaller (larger) loss rates, at least at early times.

Figure 2 suggests that both functional forms of the anomalous diffusion coefficients are able to reproduce the N -body capture rates, as long as $\mathcal{R}_1/\mathcal{R}_2$ or $\mathcal{R}_3/\mathcal{R}_4$ are not too different from one. The best correspondence is achieved, in both cases, when this ratio is slightly less than one, and this result remains unchanged even when the values of $\mathcal{R}_2(\mathcal{E})$ or $\mathcal{R}_4(\mathcal{E})$ are substantially modified. Recall that $\mathcal{R}_1 < \mathcal{R}_2$ or $\mathcal{R}_3 < \mathcal{R}_4$ imply $D_{\mathcal{R}} < 0$, i.e. $\phi_{\mathcal{R}} > 0$, i.e. a drift toward larger \mathcal{R} (Equation 37).

Changing the parameter n in the power-law diffusion coefficients from $n = 8$ to $n = 32$ had almost no discernible effect on the loss rates. Varying $\ln \Lambda$ or r_{1c}/r_g in the amounts described above did result in noticeable changes, but by amounts comparable with the ranges shown in Figure 2 due to variations in the definition of \mathcal{R}_2 or \mathcal{R}_4 . In every set

of integrations, correspondence with the N -body loss rates was best for $\mathcal{R}_1/\mathcal{R}_2 \lesssim 1$ or $\mathcal{R}_3/\mathcal{R}_4 \lesssim 1$.

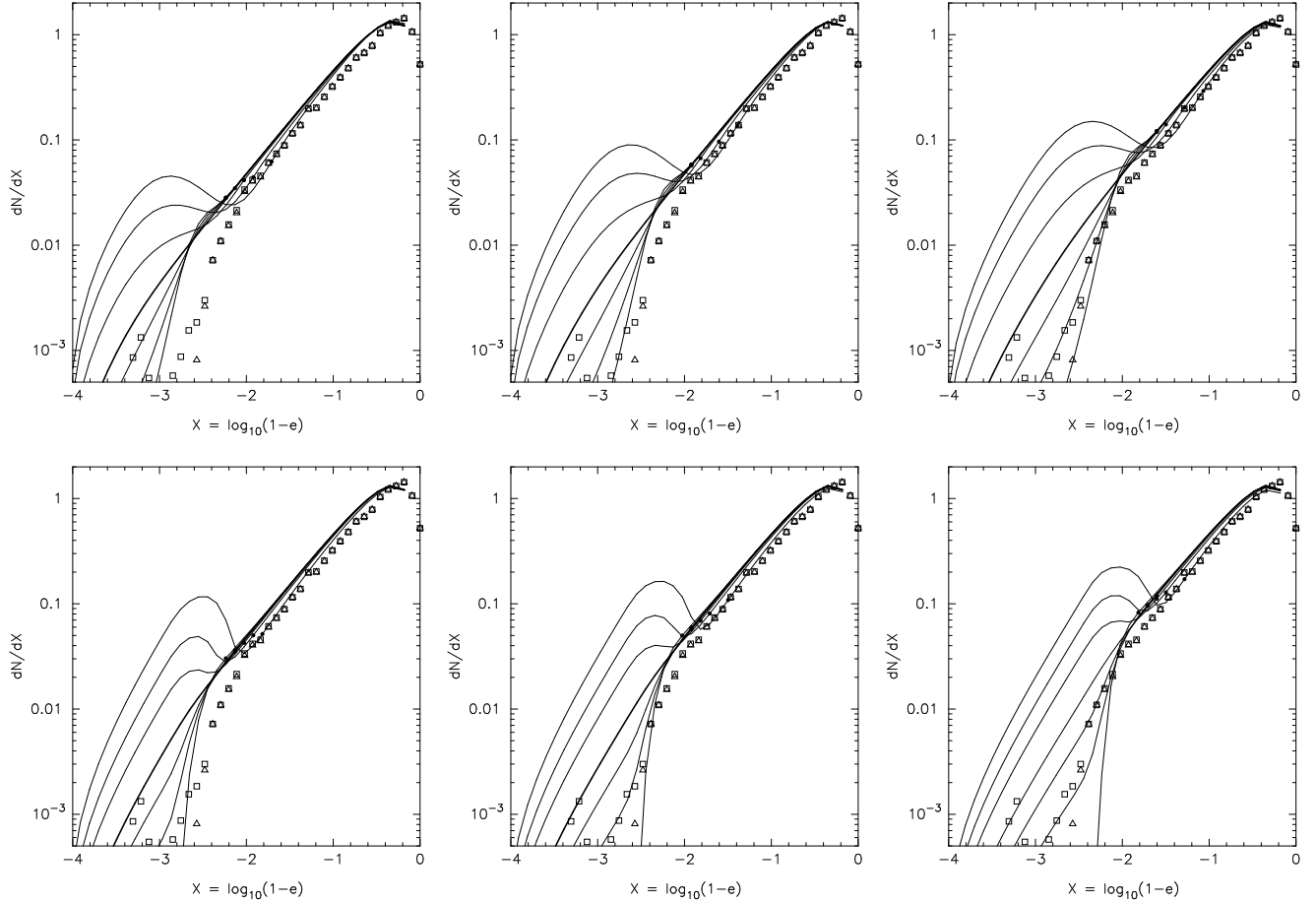


FIG. 3.— Time-averaged angular momentum distributions for stars at a single energy. The symbols are from the N -body integrations of Merritt et al. (2011) (Figure 11 from that paper); the triangles exclude stars that eventually became EMRIs while the squares include those stars. Curves were extracted from Fokker-Planck integrations that used the power-law (top) or exponential (bottom) forms of the anomalous diffusion coefficients; the curves show $f(\mathcal{R}; \mathcal{E}_4)$ where \mathcal{E}_4 is the energy corresponding to orbits of semimajor axis 4 mpc. The N -body data were computed using stars with instantaneous a values in a range $\Delta \log_{10} a = \pm 0.05$ centered on $a = 4$ mpc. Curves are distinguished by the value of $\mathcal{R}_1/\mathcal{R}_2 = \{0.7, 0.8, 0.9, 1, 1.2, 1.5, 2\}$ (top) or $\mathcal{R}_3/\mathcal{R}_4 = \{0.7, 0.9, 0.95, 1, 1.1, 1.2, 1.4\}$ (bottom); the larger this ratio, the larger the value of f at small X . The middle panel used $\mathcal{R}_2 = \mathcal{R}_{\text{SB}}^{(ii)}$ or $\mathcal{R}_4 = \mathcal{R}_{\text{SB}}^{(ii)}$. Left and right panels used $\mathcal{R}_2 = \mathcal{R}_{\text{SB}}^{(ii)}/2$ and $\mathcal{R}_2 = \mathcal{R}_{\text{SB}}^{(ii)} \times 2$ respectively (top) or $\mathcal{R}_4 = \mathcal{R}_{\text{SB}}^{(ii)}/\sqrt{\pi}$ and $\mathcal{R}_4 = \mathcal{R}_{\text{SB}}^{(ii)} \times \sqrt{\pi}$ (bottom). Filled circles mark $\mathcal{R} = \mathcal{R}_2$ (top) or $\mathcal{R} = \mathcal{R}_4$ (bottom).

Figure 3 makes another comparison between Fokker-Planck and N -body models. Plotted there are time-averaged angular momentum distributions at a single energy. These are displayed as dN/dX , where X is defined as in Figure 11 of Merritt et al. (2011):

$$X \equiv \log_{10}(1 - e) \quad (46)$$

with $e = \sqrt{1 - \mathcal{R}}$ the orbital eccentricity. Figure 3 implies that values of $\mathcal{R}_1/\mathcal{R}_2$ or $\mathcal{R}_3/\mathcal{R}_4$ of unity (“zero drift”) or greater can be securely ruled out – consistent with Figure 2. In the case of the power-law forms of the diffusion coefficients (upper panels), the best correspondence with the N -body results seems to occur for

$$\mathcal{R}_2 \approx 2\mathcal{R}_{\text{SB}}^{(ii)}, \quad 0.8 \lesssim \mathcal{R}_1/\mathcal{R}_2 \lesssim 0.9. \quad (47)$$

In the case of the exponential forms of the diffusion coefficients (lower panels), correspondence with the N -body results seems to require

$$\mathcal{R}_2 \approx \sqrt{\pi} \mathcal{R}_{\text{SB}}^{(ii)}, \quad 0.9 \lesssim \mathcal{R}_1/\mathcal{R}_2 \lesssim 0.95. \quad (48)$$

Once again, the best correspondence is achieved with diffusion coefficients that imply a non-zero drift, in the direction of increasing \mathcal{R} , in the anomalous regime.

Figure 4 shows representative plots of $f(\mathcal{R}; \mathcal{E})$ at one \mathcal{E} from the Fokker-Planck models at the final time step (roughly 2.5×10^6 yr). Dashed curves show models having parameters similar to those found to correspond best to the N -body

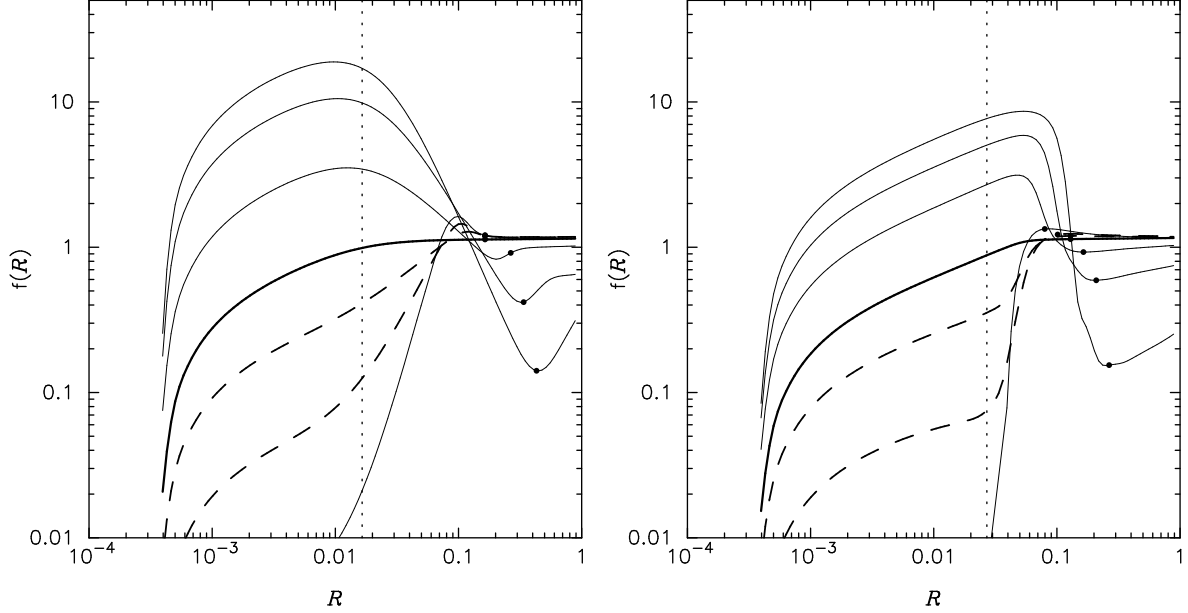


FIG. 4.— Plots of $f(\mathcal{R})$ at the final time step of the Fokker-Planck integrations described in §3.3, for stars at a single energy, corresponding to orbits with semimajor axes of 4 mpc. The left panel shows integrations based on the power-law form of the anomalous diffusion coefficients; the right panel is based on the exponential form. On the left, the parameter $\mathcal{R}_2 = 2\mathcal{R}_{\text{SB}}^{(ii)}$, and the different curves correspond to $\mathcal{R}_1/\mathcal{R}_2 = \{0.7, 0.8, 0.9, 1, 1.2, 1.5, 2\}$; the larger this ratio, the larger the value of f at small \mathcal{R} . On the right, $\mathcal{R}_4 = \sqrt{\pi}\mathcal{R}_{\text{SB}}^{(ii)}$ and $\mathcal{R}_3/\mathcal{R}_4 = \{0.7, 0.9, 0.95, 1, 1.1, 1.2, 1.4\}$. The thick solid curves in both panels are for $\mathcal{R}_1/\mathcal{R}_2 = 1$. The dashed curves show models that were judged to best reproduce the N -body data, based on results like those in Figures 2 and 3. Filled circles mark $\mathcal{R} = \mathcal{R}_{\text{SB}}$; vertical dotted lines show the values of \mathcal{R} below which classical relaxation is expected to dominate anomalous relaxation at this energy (Eqs. 51 and 53).

results. These solutions always exhibit a rapid drop in the steady-state $f(\mathcal{R})$ below the Schwarzschild barrier. That drop would be even steeper in the absence of classical relaxation, which dominates the evolution in \mathcal{R} at small \mathcal{R} (the region below the vertical dotted lines in the figure), thus maintaining a relatively high diffusion rate at small \mathcal{R} .

One final argument can be made in support of diffusion coefficients that satisfy $D_{\mathcal{R}} < 0$. As described in Antonini & Merritt (2013), stars orbiting near the Schwarzschild barrier are observed to exhibit a “buoyancy” phenomenon: should they cross the barrier from below ($\mathcal{R} < \mathcal{R}_{\text{SB}}$) to above ($\mathcal{R} > \mathcal{R}_{\text{SB}}$), they tend to remain above, and vice-versa. This behavior is consistent with a drift toward larger \mathcal{R} , as implied by $D_{\mathcal{R}} < 0$.

3.4. Dominance of classical relaxation at small \mathcal{R}

In the regime of anomalous relaxation ($\mathcal{R} < \mathcal{R}_{\text{SB}}(\mathcal{E})$), timescales for angular momentum diffusion become long for small \mathcal{R} . One consequence is that *classical* relaxation, which (by assumption) is not affected by precession, can once again dominate the evolution in angular momentum (Hamers, Portegies Zwart & Merritt 2014).

We estimate the value of \mathcal{R} at which this occurs by equating the first and second terms on the right hand sides of Equation (24). We simplify the expressions by using the limiting forms of the diffusion coefficients as $\mathcal{R} \rightarrow 0$.

For the classical diffusion coefficients, Equations (11) and (12) from Hamers, Portegies Zwart & Merritt (2014), together with the transformation Equations (32) from Paper I, yield

$$\langle \Delta \mathcal{R} \rangle_{\text{CK}} \rightarrow A^H(\mathcal{E}), \quad \langle (\Delta \mathcal{R})^2 \rangle_{\text{CK}} \rightarrow 2\mathcal{R}A^H(\mathcal{E}), \quad (49a)$$

$$A^H(a) = \frac{\ln \Lambda}{C_{\text{NRR}}(\gamma)} \left(\frac{m_{\star}}{M_{\bullet}} \right)^2 \frac{N(a)}{P(a)} \quad (49b)$$

where the symbol “ \rightarrow ” denotes the limit of small \mathcal{R} and the function $C_{\text{NRR}}(\gamma)$ is given in Appendix B of Hamers et al. (2014); their calculation assumes $\rho(r) \propto r^{-\gamma}$.

For the anomalous diffusion coefficients, Equations (24), (25) and (15) give the limiting forms

$$\langle \Delta \mathcal{R} \rangle_{\text{AR}} \rightarrow 6A(\mathcal{E}) \left(\frac{\mathcal{R}}{\mathcal{R}_1} \right)^2, \quad \langle (\Delta \mathcal{R})^2 \rangle_{\text{AR}} \rightarrow 4A(\mathcal{E})\mathcal{R} \left(\frac{\mathcal{R}}{\mathcal{R}_2} \right)^2 \quad (50)$$

in the power-law case, with $A(a)$ defined in Equation (15). Equating $\langle \Delta \mathcal{R} \rangle_{\text{CK}}$ with $\langle \Delta \mathcal{R} \rangle_{\text{AR}}$ or $\langle (\Delta \mathcal{R})^2 \rangle_{\text{CK}}$ with

$\langle(\Delta\mathcal{R})^2\rangle_{\text{AR}}$ yields

$$\frac{\mathcal{R}^2}{\mathcal{R}_1^2} = \frac{\ln \Lambda}{6 C_{\text{NR}} \alpha^2} \frac{P}{t_{\text{coh}}} \quad (\text{1st order}), \quad (51a)$$

$$\frac{\mathcal{R}^2}{\mathcal{R}_2^2} = \frac{\ln \Lambda}{2 C_{\text{NR}} \alpha^2} \frac{P}{t_{\text{coh}}} \quad (\text{2nd order}). \quad (51b)$$

Replacing \mathcal{R}_1 and \mathcal{R}_2 by $\mathcal{R}_{\text{SB}}^{(ii)}$ in Eqs. (51) and setting $\alpha = 1.6$ yields

$$\mathcal{R}^2 = (1.0, 3.1) \frac{\ln \Lambda}{C_{\text{NR}}} \left(\frac{r_g}{a}\right)^2 \frac{t_{\text{coh}}}{P} \quad (52)$$

where the constants in parentheses refer to first- and second-order diffusion coefficients respectively. Equation (52) is similar to Equation (23a) of Hamers, Portegies Zwart & Merritt (2014).

Equations (51) were used to plot the vertical dotted lines in the left-hand panels of Figures 1 and 4 (note that these two figures refer to different mass models). In Figure 1, the line predicts reasonably well the value of \mathcal{R} at which the data begin to deviate from the fitted curves. In the case of Figure 4, the effects of classical relaxation can be seen in the steady-state $f(\mathcal{R})$, which drops more gradually to zero below the SB than it would if only anomalous relaxation were acting (Figure 10).

If the exponential forms of the anomalous diffusion coefficients are correct, then the value of \mathcal{R} at which $\langle(\Delta\mathcal{R})^2\rangle_{\text{CK}} = \langle(\Delta\mathcal{R})^2\rangle_{\text{AR}}$ becomes

$$\frac{\mathcal{R}^2}{\mathcal{R}_4^2} = \left[\log \left(\frac{2\alpha^2 C_{\text{NR}} t_{\text{coh}}}{\ln \Lambda} \frac{t_{\text{coh}}}{P} \right) \right]^{-1}. \quad (53)$$

This value for \mathcal{R} is plotted, in addition to the value given by Equation (52), on the lower right-hand panel of Figure 1. Note that under this hypothesis, the range in \mathcal{R} over which anomalous relaxation would be relevant would become very small; in effect, classical relaxation would dominate the evolution everywhere below (and sometimes even above) the Schwarzschild barrier. We reiterate that there is no support for the exponential form of the anomalous diffusion coefficients in any published numerical simulations.

4. STEADY-STATE SOLUTIONS

Paper II presented steady-state solutions for $f(\mathcal{E}, \mathcal{R})$ obtained via integrations of the Fokker-Planck equation with diffusion coefficients given by Equation (13) (no anomalous relaxation) and outer boundary condition

$$f^*(\mathcal{E}_{\text{min}}^*, \mathcal{R}^*, t^*) = f^*(\mathcal{E}_{\text{min}}^*, \mathcal{R}^*, 0) \quad (54)$$

with f the phase-space density and \mathcal{E}_{min} the minimum value of \mathcal{E} on the energy grid. (Asterisks denote dimensionless quantities; see Equation 12 and Paper I.) Initial conditions for f were based on an isotropic power-law model, $n \propto r^{-7/4}$, $f \propto \mathcal{E}^{1/4}$, but with a simple modification to account for the presence of the loss cone:

$$f(\mathcal{E}, \mathcal{R}, t = 0) = 0, \quad \mathcal{R} \leq \mathcal{R}_{\text{lc}}(\mathcal{E}). \quad (55)$$

Among the parameters that were varied in the integrations of Paper II were m_*/M_\bullet and the initial density at large radii; the latter was chosen to have one of three values, bracketing the estimated value for the nucleus of the Milky Way. The physical radius of the loss sphere, r_{lc} , was fixed at $15r_g = 15GM_\bullet/c^2$, roughly the tidal disruption radius of a solar-type star.

We repeated a subset of those integrations, now using the modified expressions for the angular-momentum diffusion coefficients that account for anomalous relaxation: either power-law (Equation 24) or exponential (Equation 40).

The dimensionless parameter m_*/M_\bullet was set to 2.5×10^{-7} . Assuming $M_\bullet = 4 \times 10^6 M_\odot$, the (dimensional) stellar mass becomes $m_* = 1.0 M_\odot$. The outer boundary condition was chosen, as in Paper II, to give one of the following three values for the mass density at one parsec:

$$\{1.9 \times 10^4, 3.5 \times 10^5, 6.1 \times 10^6\} M_\odot \text{pc}^{-3} \quad (56)$$

where again $M_\bullet = 4 \times 10^6 M_\odot$ has been assumed. For each of these parameter choices, two other parameters that appear in the expressions for the anomalous diffusion coefficients were varied:

1. $\mathcal{R}_1/\mathcal{R}_2$ (power-law) or $\mathcal{R}_3/\mathcal{R}_4$ (exponential) ;
2. The ratio $\mathcal{R}_2/\mathcal{R}_{\text{SB}}$ or $\mathcal{R}_4/\mathcal{R}_{\text{SB}}$.

Based on the results described in the previous section, the following parameter values were considered:

- $\mathcal{R}_1/\mathcal{R}_2 = \{0.8, 1.0, 1.2\}$; $\mathcal{R}_3/\mathcal{R}_4 = \{0.9, 1.0, 1.1\}$
- $\mathcal{R}_2/\mathcal{R}_{\text{SB}} = \{0.5, 1.0, 2.0\}$; $\mathcal{R}_4/\mathcal{R}_{\text{SB}} = \{0.5, 1.0, 2.0\}$.

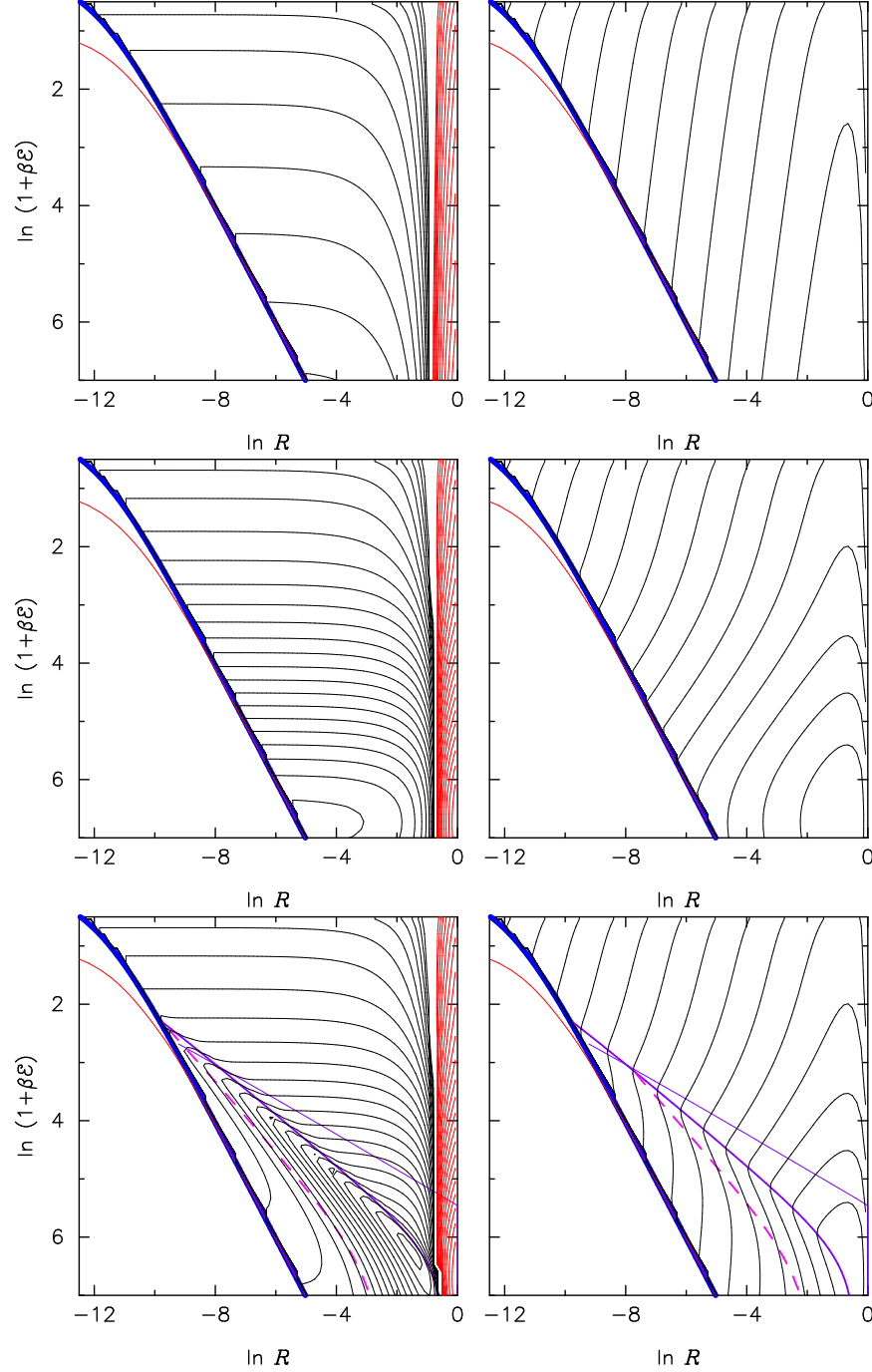


FIG. 5.— Angular momentum diffusion coefficients at $t = 0$ in the models of §4. **Top:** $\langle \Delta \mathcal{R} \rangle_{\text{CK}}$ (left), $\langle (\Delta \mathcal{R})^2 \rangle_{\text{CK}}$ (right). **Middle:** $\langle \Delta \mathcal{R} \rangle_{\text{CK}} + \langle \Delta \mathcal{R} \rangle_{\text{RR}}$ (left), $\langle (\Delta \mathcal{R})^2 \rangle_{\text{CK}} + \langle (\Delta \mathcal{R})^2 \rangle_{\text{RR}}$ (right). **Bottom:** Modified forms of the diffusion coefficients that account for anomalous relaxation, Equations (24), with parameters as given in the text. The physical loss cone radius is shown as the thick (blue) curve in each panel; $f = 0$ is assumed inside this curve at $t = 0$ (“empty loss cone”). The thin (red) curve that lies inside the loss cone is the quantity $\mathcal{R}_0(\mathcal{E})$ defined in Paper I. In the panels showing $\langle \Delta \mathcal{R} \rangle$, the red contours indicate $-\langle \Delta \mathcal{R} \rangle$, i.e. $\langle \Delta \mathcal{R} \rangle < 0$ in these regions. In the lower panels, two expressions for the location of the Schwarzschild barrier, $\mathcal{R}_{\text{SB}}^{(i)}(\mathcal{E})$ and $\mathcal{R}_{\text{SB}}^{(ii)}(\mathcal{E})$, are shown respectively as the thin and thick magenta curves. The dashed curves in the lower panels indicate where the timescales for classical and anomalous relaxation are equal. Contour values are the same in all frames.

For $\mathcal{R}_{\text{SB}}(\mathcal{E})$, the expression (18) was used. The parameter n that appears in the power-law form of the anomalous diffusion coefficients was set to 8 in all integrations.

Figure 5 plots the diffusion coefficients $\langle \Delta \mathcal{R} \rangle$, $\langle (\Delta \mathcal{R})^2 \rangle$ as computed by the code at $t = 0$, in models having the middle of the three values for the mass density at one parsec (Equation 56). The top two frames plot the classical diffusion coefficients:

$$\langle \Delta \mathcal{R} \rangle_{\text{CK}}, \quad \langle (\Delta \mathcal{R})^2 \rangle_{\text{CK}}.$$

The middle two frames plot diffusion coefficients that account for resonant relaxation:

$$\langle \Delta \mathcal{R} \rangle_{\text{CK}} + \langle \Delta \mathcal{R} \rangle_{\text{RR}}, \quad \langle (\Delta \mathcal{R})^2 \rangle_{\text{CK}} + \langle (\Delta \mathcal{R})^2 \rangle_{\text{RR}}.$$

These are the same expressions adopted in the integrations of Paper I. The lower set of frames show the diffusion coefficients of Equation (24), which account for anomalous relaxation (power-law modification, with $n = 8$, $\mathcal{R}_2 = 2\mathcal{R}_{\text{SB}}^{(ii)}$, and $\mathcal{R}_1 = \mathcal{R}_2$). In the case of the exponential modification (not shown in this figure), the diffusion coefficients drop off more steeply below the Schwarzschild barrier. However, this drop is mediated, in all models, by the presence of classical diffusion, which dominates again at sufficiently small \mathcal{R} , as discussed above.

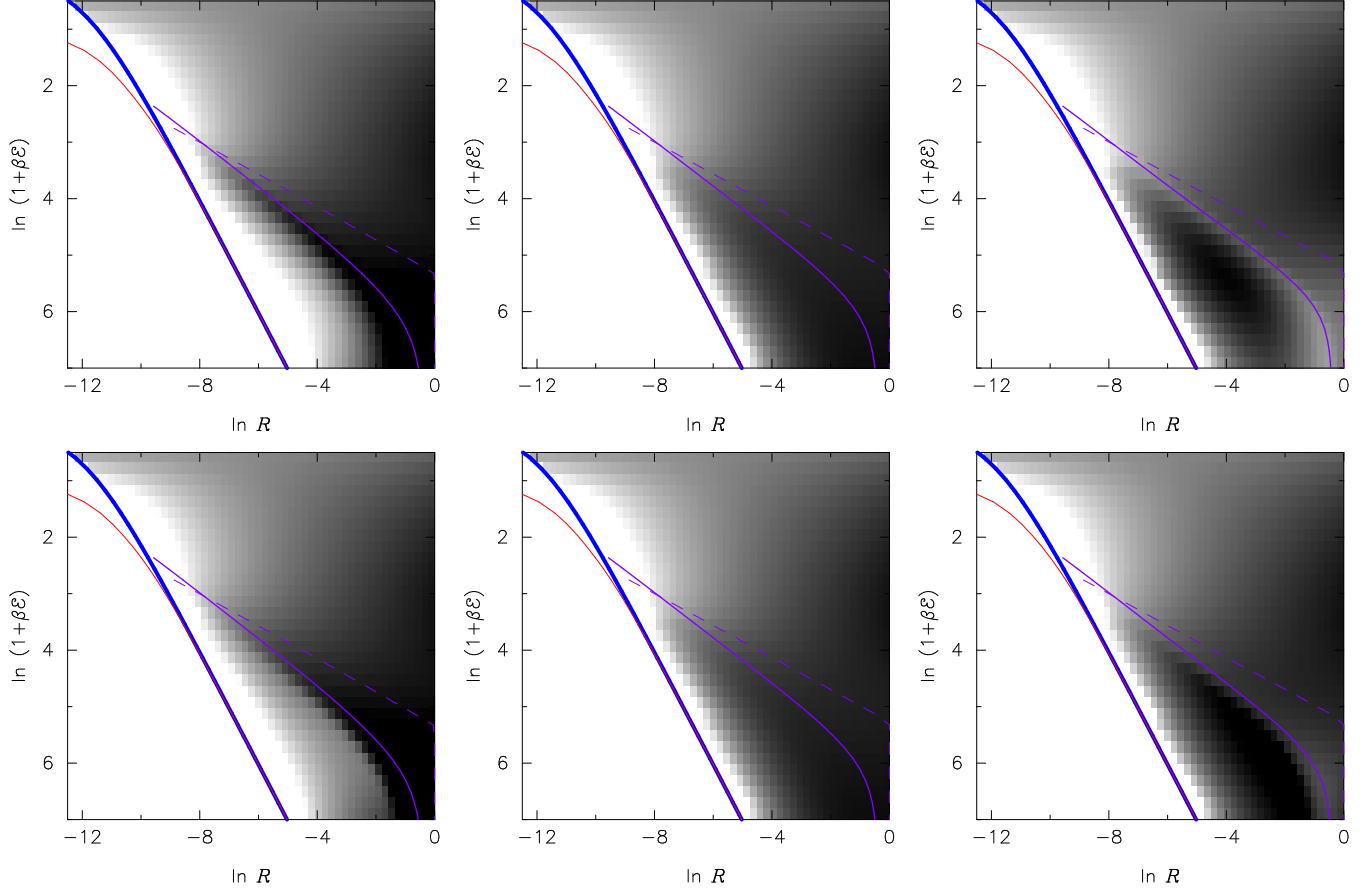


FIG. 6.— Grey-scale of $\log f^*$ in a set of six, steady-state models. **Top:** models integrated using the power-law forms of the anomalous diffusion coefficients, with $\mathcal{R}_2/\mathcal{R}_{\text{SB}} = 2$, and with $\mathcal{R}_1/\mathcal{R}_2 = 0.8$ (left), 1.0 (middle) and 1.2 (right). **Bottom:** models integrated using the exponential forms of the anomalous diffusion coefficients, with $\mathcal{R}_4/\mathcal{R}_{\text{SB}} = 2$, and with $\mathcal{R}_3/\mathcal{R}_4 = 0.9$ (left), 1.0 (middle) and 1.1 (right). Other parameters are given in the text. Curves have the same meaning as in Figure 5.

Steady-state solutions, $f^*(\mathcal{E}^*, \mathcal{R}^*)$, are shown in Figure 6, again for models with $\rho(1\text{pc}) \approx 3.5 \times 10^6 M_\odot \text{pc}^{-3}$. The top(bottom) panels show solutions obtained using the power-law(exponential) expressions for the anomalous diffusion coefficients, with $\mathcal{R}_2/\mathcal{R}_{\text{SB}} = 2$ or $\mathcal{R}_4/\mathcal{R}_{\text{SB}} = 2$. What varies, from left to right, is the choice of $\mathcal{R}_1/\mathcal{R}_2$ (top) or $\mathcal{R}_3/\mathcal{R}_4$ (bottom). When these ratios are unity (“zero-drift”), the steady-state solutions are characterized by $f(\mathcal{R}) \sim \text{constant}$ near the SB. When these ratios are greater or less than one, the steady-state solutions behave in roughly the way seen in Figures 4 and 10, becoming either greater or smaller in the region below the Schwarzschild barrier, before dropping to zero at the loss cone boundary. Evidently, the form of the steady-state f in this region depends very sensitively on deviations of that ratio from unity. Depending on the value of that ratio, f in the region below the barrier can either be strongly depleted, or strongly enhanced, compared with the “zero-drift” solution.

Angular-momentum-averaged distribution functions, defined as

$$\bar{f}(\mathcal{E}) \equiv \int_{\mathcal{R}_{\text{lc}}(\mathcal{E})}^1 f(\mathcal{E}, \mathcal{R}) d\mathcal{R}, \quad (57)$$

are plotted in Figure 7 for all of the steady-state solutions. Shown for comparison, as the thick solid curves, are \bar{f} for models computed without anomalous diffusion; these are the same three curves plotted in Figure 5 of Paper II. As discussed in that paper, inclusion of the resonant diffusion coefficients has the effect of sharply truncating the

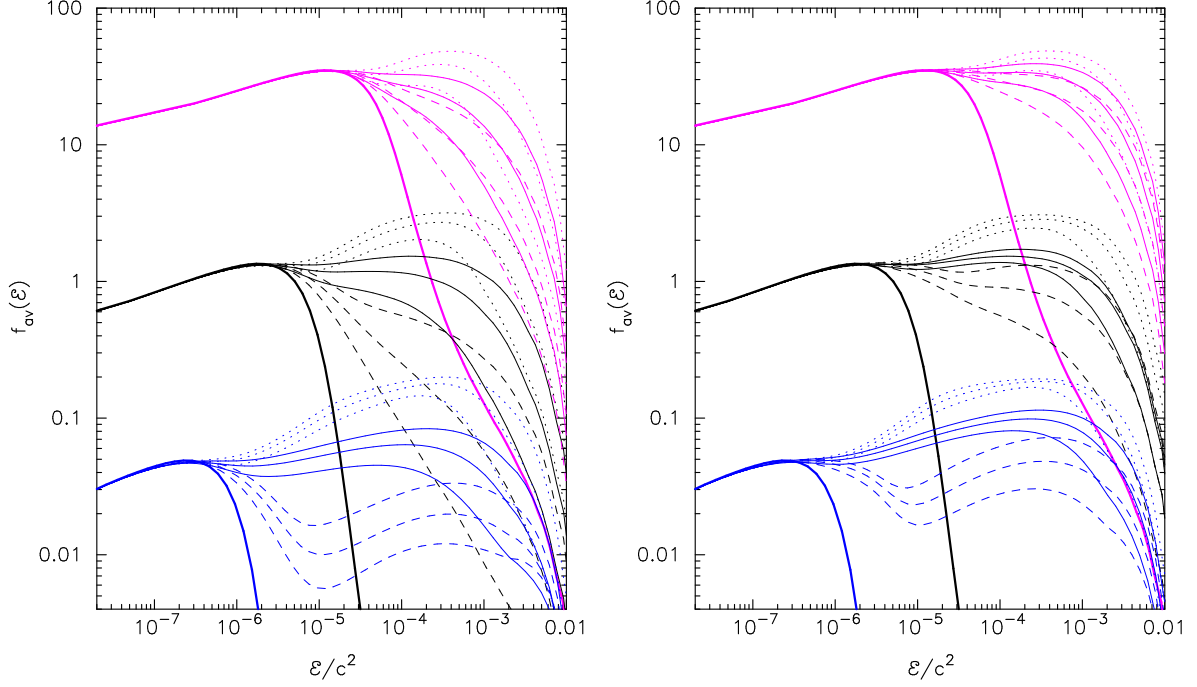


FIG. 7.— Angular-momentum-averaged distribution functions, $\bar{f}(\mathcal{E})$, for all of the steady-state models; left(right) panel used the power-law(exponential) forms of the anomalous diffusion coefficients. The three values of the large-radius density normalization, Equation (56), are indicated by the three colors (high density, magenta; intermediate density, black; low density, blue). In each of the three sets of models, the solid curves have $\mathcal{R}_1/\mathcal{R}_2 = 1$ (left) or $\mathcal{R}_3/\mathcal{R}_4 = 1$ (right); the dashed curves have $\mathcal{R}_1/\mathcal{R}_2 = 1.2$ (left) or $\mathcal{R}_3/\mathcal{R}_4 = 1.1$ (right); the dotted curves have $\mathcal{R}_1/\mathcal{R}_2 = 0.8$ (left) or $\mathcal{R}_3/\mathcal{R}_4 = 0.9$ (right). For each choice of these parameters, there are three curves, with the same line style, corresponding to the three choices $\{0.5, 1.0, 2.0\}$ for $\mathcal{R}_2/\mathcal{R}_{\text{SB}}$ or $\mathcal{R}_4/\mathcal{R}_{\text{SB}}$. The three thick, solid curves in each panel are from integrations that did not account for anomalous relaxation; these are the same curves plotted in Figure 5 of Paper II.

steady-state $\bar{f}(\mathcal{E})$, at binding energies above a certain value, where the timescale for resonant diffusion (in angular momentum) drops below the timescale for classical diffusion (in energy), and stars are carried rapidly into the SBH. The truncation of \bar{f} can still be seen in the new models; but it is mediated by the presence of anomalous relaxation. The reason is the increase in the angular-momentum diffusion time when anomalous relaxation is accounted for: stars “pile up” near the Schwarzschild barrier, until their density is high enough to drive the requisite flux.

Closely related to $\bar{f}(\mathcal{E})$ is $\rho(r)$, the mass density. Figure 8 shows steady-state density profiles for all the integrations. Also shown are three density profiles from Figure 4 of Paper II (no anomalous relaxation), which exhibit cores corresponding to the depletion in $\bar{f}(\mathcal{E})$ at large binding energies due to resonant relaxation. Once again, the lesser depletion in the models that account for anomalous relaxation translates into cores of lesser prominence. Indeed in the models with $\mathcal{R}_1 < \mathcal{R}_2$ or $\mathcal{R}_3 < \mathcal{R}_4$, the steady-state density profiles turn out to be very close to the classical Bahcall-Wolf cusp at all radii plotted. This plot confirms a conjecture made in Paper I: namely: that the inhibition in angular-momentum diffusion associated with the Schwarzschild barrier would reduce the ability of resonant relaxation to form a core. The generality of this result is discussed in §5.

Even models having similar $\rho(r)$ or $\bar{f}(\mathcal{E})$ can have very different loss rates into the SBH, since the latter depends also on the timescale for angular-momentum diffusion. The flux of stars into the loss cone, Equation (5), is plotted for the steady-state models as a function of energy in Figure 9. Shown for comparison are loss rates in steady-state models computed using only classical, or classical plus resonant, relaxation. These plots show that the flux of stars into the SBH can depend strongly on the assumed forms of the anomalous diffusion coefficients. There are two, competing effects. Including anomalous relaxation tends to increase the steady-state density at small radii compared to $\rho(r)$ computed using resonant relaxation alone, resulting in a larger flux. Anomalous relaxation also increases the timescales for angular momentum diffusion, which tends to reduce the flux.

The dependence of the flux on the assumed value of $\mathcal{R}_1/\mathcal{R}_2$ or $\mathcal{R}_3/\mathcal{R}_4$ is similarly complex. At low binding energies, Figure 9 shows that small values of this ratio imply lower fluxes; while at high binding energies, the reverse is true. The former result is consistent with the analysis in the Appendix (Figure 11). The reason for the latter result can be seen in Figure 7: models with smaller values of this ratio maintain larger \bar{f} at large binding energies, which tends to increase the flux. **Total, or integrated, loss rates for these models can be computed using Equation (8). The results turn out to be nearly the same – within a few percent – for each of the models, roughly 7×10^{-4} stars per year. As discussed in Paper I, this is a consequence of the fact that the total loss rate is dominated by stars at low binding energies, where the effects of resonant and anomalous relaxation are small.**

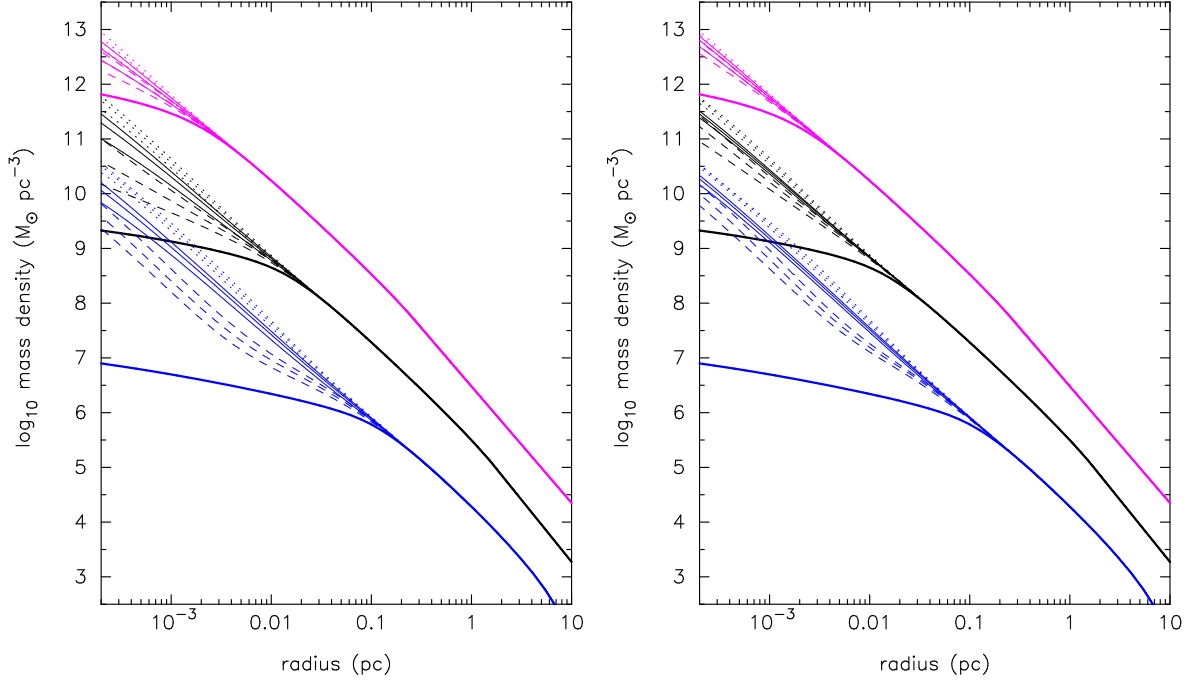


FIG. 8.— Mass density as a function of radius for the steady-state models. Line colors and line styles have the same meanings as in Figure 7. Scaling to physical units assumes $M_{\bullet} = 4 \times 10^6 M_{\odot}$.

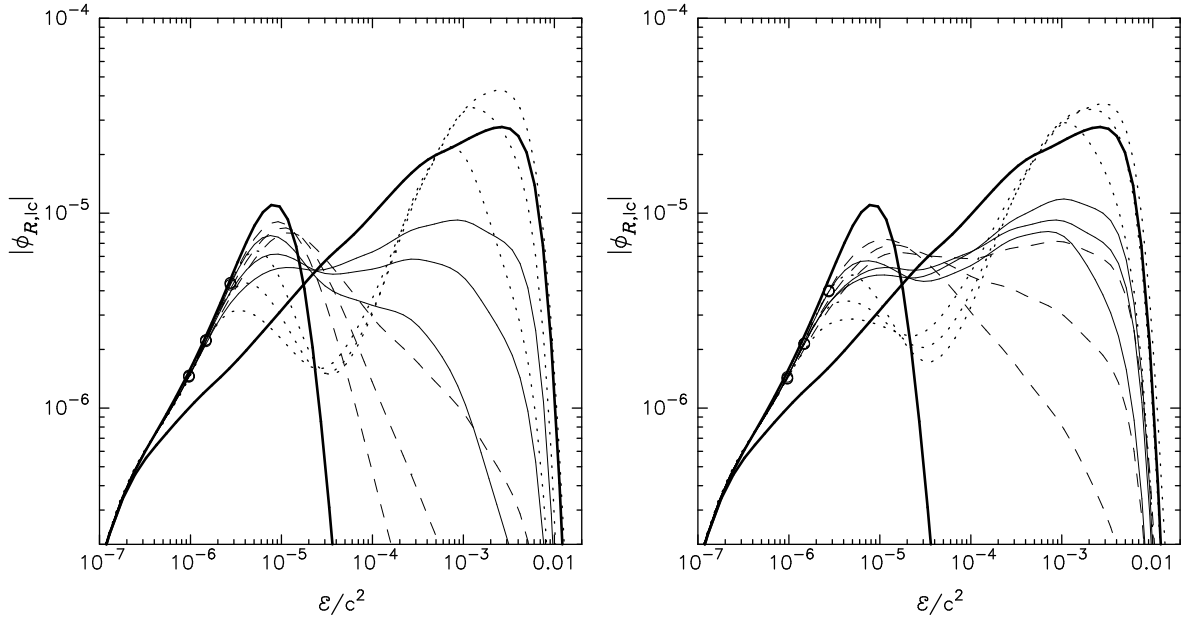


FIG. 9.— Dimensionless flux of stars into the loss cone as a function of energy in the steady-state models; all of these models used the intermediate of the three values given in Equation (56) for the density at one parsec. Left(right) panels adopted the power-law(exponential) forms of the anomalous diffusion coefficients. The two, thick solid curves in each panel show models that included only classical relaxation (curves that peak near the right) and only classical plus resonant relaxation (curves that peak near the left). Line styles have the same meanings as in Figures 7 and 8. Circles are plotted at values of \mathcal{E} corresponding to the outer edge of the Schwarzschild barrier.

5. DISCUSSION

5.1. Steady-state density profiles

In Paper II, the formation of cores due to resonant relaxation was discussed. Equation (38) of that paper gave an estimate of the radius of the core so formed:

$$\frac{a_{\text{core}}}{r_m} \approx 0.028 \left(\frac{\ln \Lambda}{15} \right)^{-4/5}. \quad (58)$$

Here, r_m is the gravitational influence radius of the SBH, defined as the radius of a sphere containing a mass in stars of $2M_\bullet$.

As described in this paper, at least in the case of the Milky Way, the inclusion of anomalous relaxation tends to counteract core formation by causing stars to accumulate near the Schwarzschild barrier.

Here we consider the generality of that result. Suppose that nuclei of galaxies fainter than the Milky Way have SBHs that satisfy the $M_\bullet - \sigma$ relation:

$$\frac{M_\bullet}{10^6 M_\odot} \approx 5.76 \left(\frac{\sigma}{100 \text{ km s}^{-1}} \right)^{4.86}$$

(Merritt 2013, Eq. 2.33) and that their nuclear densities are close to the Bahcall-Wolf form, $\rho(r) \propto r^{-7/4}$. The latter is not too different from $\rho \propto r^{-2}$, for which $r_m \approx r_h \equiv GM_\bullet/\sigma^2$. Under these assumptions,

$$r_m \approx 0.88 \left(\frac{M_\bullet}{10^6 M_\odot} \right)^{0.59} \text{ pc}, \quad M_\bullet \lesssim 4 \times 10^6 M_\odot. \quad (59)$$

We first verify the assumptions that led to Equation (58). That equation was derived assuming that $t_{\text{coh}} = t_{\text{coh,M}}$ (Equation 16). The radius at which $t_{\text{coh,M}} = t_{\text{coh,S}}$, for a nucleus with $\rho(r) \propto r^{-7/4}$, is given by Equation (30) from Paper II:

$$\frac{a_{\text{coh}}}{r_m} \approx 1.2 \times 10^{-3} \left(\frac{M_\bullet}{10^6 M_\odot} \right)^{4/9} \left(\frac{r_m}{1 \text{ pc}} \right)^{-4/9} \approx 1.3 \times 10^{-3} \left(\frac{M_\bullet}{10^6 M_\odot} \right)^{0.18} \quad (60)$$

suggesting that indeed $t_{\text{coh}} \sim t_{\text{coh,M}}$ at $a = a_{\text{core}}$ in the galaxies of interest.

Next we ask how a_{core} compares with the radii that define the Schwarzschild barrier. Equation (20) gave approximate limits on the extent of the SB in a $\rho \propto r^{-7/4}$ nucleus, which we recast here as

$$\frac{a_{\text{min}}}{r_m} \approx \left(\frac{M_\bullet}{2m_\star} \right)^{4/13} \left(\frac{r_g}{r_m} \right)^{8/13}, \quad \frac{a_{\text{max}}}{r_m} \approx (4\Theta)^{-4/9} \left(\frac{M_\bullet}{m_\star} \right)^{4/9} \left(\frac{r_g}{r_m} \right)^{4/9}. \quad (61)$$

Comparing a_{min} and a_{max} to a_{core} :

$$\frac{a_{\text{min}}}{a_{\text{core}}} \approx 29 \left(\frac{M_\bullet}{m_\star} \right)^{4/13} \left(\frac{r_g}{r_m} \right)^{8/13} \left(\frac{\ln \Lambda}{15} \right)^{4/5}, \quad (62a)$$

$$\frac{a_{\text{max}}}{a_{\text{core}}} \approx 5.8 \left(\frac{\Theta}{15} \right)^{-4/9} \left(\frac{M_\bullet}{m_\star} \right)^{4/9} \left(\frac{r_g}{r_m} \right)^{4/9} \left(\frac{\ln \Lambda}{15} \right)^{4/5}. \quad (62b)$$

Using $r_g \approx 4.78 \times 10^{-8} (M_\bullet/10^6 M_\odot) \text{ pc}$, these become

$$\frac{a_{\text{min}}}{a_{\text{core}}} \approx 0.064 \left(\frac{M_\bullet}{10^6 M_\odot} \right)^{12/13} \left(\frac{m_\star}{M_\odot} \right)^{-4/13} \left(\frac{r_m}{1 \text{ pc}} \right)^{-8/13} \left(\frac{\ln \Lambda}{15} \right)^{4/5}, \quad (63a)$$

$$\frac{a_{\text{max}}}{a_{\text{core}}} \approx 1.5 \left(\frac{\Theta}{15} \right)^{-4/9} \left(\frac{M_\bullet}{10^6 M_\odot} \right)^{8/9} \left(\frac{m_\star}{M_\odot} \right)^{-4/9} \left(\frac{r_m}{1 \text{ pc}} \right)^{-4/9} \left(\frac{\ln \Lambda}{15} \right)^{4/5}. \quad (63b)$$

Setting $a_{\text{max}} < a_{\text{core}}$ implies that anomalous relaxation is unlikely to affect the formation of the core due to resonant relaxation. This condition is:

$$r_m \gtrsim 2.5 \left(\frac{\Theta}{15} \right)^{-1} \left(\frac{M_\bullet}{10^6 M_\odot} \right)^2 \left(\frac{m_\star}{M_\odot} \right)^{-1} \left(\frac{\ln \Lambda}{15} \right)^{9/5} \text{ pc}. \quad (64)$$

In the case of the Milky Way ($M_\bullet \approx 4 \times 10^6 M_\odot$), satisfying this condition for $m_\star = M_\odot$ would require $r_m \gtrsim 40 \text{ pc}$ – about ten times larger than the value inferred from stellar kinematics. This is consistent with Figure 8, which showed that anomalous relaxation inhibits the formation of a core for all reasonable values of r_m . In the case of galaxies with central black holes less massive than the Milky Way's, Equations (64) and (59) allow us to write the condition $a_{\text{max}} < a_{\text{core}}$ as

$$M_\bullet \lesssim 5 \times 10^5 \left(\frac{\Theta}{15} \right)^{0.48} \left(\frac{m_\star}{M_\odot} \right)^{0.48} \left(\frac{\ln \Lambda}{15} \right)^{-0.86} M_\odot. \quad (65)$$

Thus, the core formed by resonant relaxation is expected to become progressively more prominent as M_\bullet is reduced below its value in the Milky Way. This fact is likely to be important in determining the rate of formation of gravitational-wave sources, particularly since theoretical estimates often focus on galaxies with $M_\bullet \lesssim 10^6 M_\odot$. Estimating this rate will be the topic of upcoming papers in this series.

5.2. Constraining the forms of the anomalous diffusion coefficients

Until recently, discussions of gravitational encounters near a SBH have usually been presented in terms of diffusion *timescales*; that is; in terms of second-order diffusion coefficients like $\langle(\Delta L)^2\rangle$ (Rauch & Tremaine 1996; Hopman & Alexander 2006a,b; Gürkan & Hopman 2007; Eilon et al. 2009; Madigan et al. 2011). Hamers, Portegies Zwart & Merritt (2014) were apparently the first to consider the forms of the first-order diffusion coefficients. Of course, both first- and second-order diffusion coefficients are essential when computing the evolution of f via the Fokker-Planck equation.

As shown here through a number of examples, the form of the steady-state $f(\mathcal{E}, \mathcal{R})$ near the Schwarzschild barrier can depend very sensitively on the relative amplitude of the first- and second-order coefficients in the anomalous-relaxation regime. A natural case to consider is that of “zero drift”, in which the two diffusion coefficients imply a net flux in angular momentum that is zero when $f(\mathcal{R}) = \text{constant}$ (§3.1). While it may be natural – it is consistent with a “maximum-entropy” steady state – this assumption is not compelled by any physical argument of which we are aware. In stellar dynamics, incorrect conclusions drawn from entropy arguments are legion, and numerical experiments, when available, would seem to be a better guide. As discussed in detail in §3.3, the highest-quality N -body simulations carried out to date of this regime (Merritt et al. 2011) seem to require anomalous diffusion coefficients that differ slightly, though significantly, from the “zero-drift” condition. A state of “positive drift” seems to better characterize the existing simulations.

Elucidation of the long-term effects of gravitational encounters in the Schwarzschild regime near a SBH will ultimately require a better specification of the anomalous diffusion coefficients. By far the best way to do this – at least in principle – is via direct N -body integrations, which impose the fewest approximations. In practice, integrations of the required accuracy become very time-consuming when $N \gtrsim 10^2$. A major effort should be devoted to increasing the efficiency of the N -body integrators.

6. SUMMARY

Integrations of the Fokker-Planck equation describing $f(E, L, t)$, the phase-space density of stars around a super-massive black hole (SBH) at the center of a galaxy, were carried out using a numerical algorithm described in two earlier papers (Merritt 2015a,b). Diffusion coefficients describing classical, resonant and “anomalous” relaxation were included; the latter accounting for the evolution of orbits in the regime below the Schwarzschild barrier (SB) where the timescale for general relativistic precession is short compared with the coherence time, invalidating the assumptions that underlie the theory of resonant relaxation (Merritt et al. 2011). The principal results follow.

1. Since a good theoretical understanding of anomalous relaxation is still lacking, two functional forms were considered for the angular momentum diffusion coefficients in this regime, having either a power-law or exponential dependence on $\mathcal{R} \equiv L^2/L_c^2$. In either case, a further choice must be made in terms of how to relate the first- and second-order diffusion coefficients. It was argued that a natural starting point is a “zero-drift” condition that implies no net flux in angular momentum when $f(\mathcal{R})$ is constant. Parameterized functional forms for $\langle\Delta\mathcal{R}\rangle$ and $\langle(\Delta\mathcal{R})^2\rangle$ were proposed that have the “zero-drift” property as a special case.

2. Two attempts were made to constrain the forms of the anomalous diffusion coefficients by comparison with published numerical simulations. First, as in Hamers, Portegies Zwart & Merritt (2014), diffusion coefficients extracted from a large set of test-particle integrations were compared with the two functional forms. The power-law form was found to be strongly preferred, at least in the case of the second-order coefficient, confirming a result already presented in that paper. The first-order coefficient was also well fit by the power-law form, although data were more noisy and no clear preference could be established for the “zero-drift” conditions. Second, a set of Fokker-Planck integrations were carried out based on the same initial conditions that were used in the exact N -body integrations of Merritt et al. (2011). Two properties of those models were then compared: the dependence of f on \mathcal{R} , and the capture rate; in both cases, results from the N -body integrations were averaged over a set of different runs to reduce noise. Both the power-law and exponential forms for the diffusion coefficients could be made consistent with these data; it was argued that this was due in part to the effects of classical relaxation, which always dominates the diffusion rate at sufficiently small \mathcal{R} . However, a clear preference was established for diffusion coefficients that imply a steady-state drift toward larger \mathcal{R} , inconsistent with the “zero-drift” hypothesis.

3. Fokker-Planck integrations were then carried out to find steady-state models having parameters similar to those of the nuclear star cluster in the Milky Way. These models were identical to the steady-state models computed in Paper II except for the inclusion of the anomalous diffusion coefficients. The steady-state $f(\mathcal{E}, \mathcal{R})$ in regions of phase space below the Schwarzschild barrier ($\mathcal{R} < \mathcal{R}_{\text{SB}}$) was found to be most strongly dependent on the assumed relation between first- and second-order diffusion coefficients. Diffusion coefficients satisfying the “zero-drift” condition produced steady-state solutions in which f was nearly constant with respect to \mathcal{R} below the SB. Integrations incorporating positive- or negative-drift diffusion coefficients had steady-state f ’s that respectively increased or decreased below the SB, before falling to zero at the loss cone boundary. In all of these models, departures of the steady-state density, $n(r)$, from the classical Bahcall-Wolf solution were less pronounced than in the models of Paper II that did not incorporate anomalous relaxation (a result that was suggested already in that paper). The reason is the tendency of stars to accumulate near and below the SB, thus counteracting the depletion that occurs when only resonant relaxation is accounted for.

4. Steady-state loss rates in the presence of anomalous relaxation differ from those in all models previously published, for two reasons: different steady-state phase-space densities, and different forms of the angular-momentum diffusion coefficients. A robust conclusion is that the incorporation of anomalous relaxation implies a lower capture rate at energies where the SB exists, compared with models that only incorporate resonant relaxation, and this is true in spite of the generally higher steady-state densities in the former models. However the reduction in the capture rate depends sensitively on the parameters adopted for the anomalous diffusion coefficients, being most(least) extreme for the positive-(negative-) drift cases.

5. In galaxies with SBHs less massive than the Milky Way's, core formation by resonant relaxation is likely to be progressively less affected by anomalous relaxation.

A. Hamers kindly provided data from his TPI code that were used in constraining the functional forms of the anomalous diffusion coefficients in §3. I also thank him, F. Antonini and E. Vasiliev for comments that improved the manuscript. This work was supported by the National Science Foundation under grant no. AST 1211602 and by the National Aeronautics and Space Administration under grant no. NNX13AG92G.

APPENDIX

Properties of steady-state solutions in the anomalous-relaxation regime

We consider solutions to the time-independent Fokker-Planck equation in \mathcal{R} -space in the anomalous-relaxation regime. We assume that the diffusion coefficients are modified versions of the resonant diffusion coefficients:

$$\langle \Delta \mathcal{R} \rangle = w_1(\mathcal{E}, \mathcal{R}) \langle \Delta \mathcal{R} \rangle_{\text{RR}}, \quad \langle (\Delta \mathcal{R})^2 \rangle = w_2(\mathcal{E}, \mathcal{R}) \langle (\Delta \mathcal{R})^2 \rangle_{\text{RR}}, \quad (\text{A1a})$$

$$\langle \Delta \mathcal{R} \rangle_{\text{RR}} = 2A(\mathcal{E}) (1 - 2\mathcal{R}) g_1(\mathcal{E}, \mathcal{R}), \quad \langle (\Delta \mathcal{R})^2 \rangle_{\text{RR}} = 4A(\mathcal{E}) \mathcal{R} (1 - \mathcal{R}) g_2(\mathcal{E}, \mathcal{R}) \quad (\text{A1b})$$

and consider the two functional forms for $\{w_1, w_2\}$ that were considered in §3: a power-law modification, and an exponential modification. Diffusion in energy is ignored.

(1) Power-law

Identify w_1 and w_2 with g_1 and g_2 given respectively by Equations (33) and (25):

$$g_1(\mathcal{E}, \mathcal{R}) = \left\{ 1 + \left[\frac{R_1(\mathcal{E})}{\mathcal{R}} \right]^n \right\}^{-2/n} + \frac{2(1 - \mathcal{R})}{1 - 2\mathcal{R}} \left(\frac{\mathcal{R}_1}{\mathcal{R}} \right)^n \left\{ 1 + \left[\frac{R_1(\mathcal{E})}{\mathcal{R}} \right]^n \right\}^{-2/n-1},$$

$$g_2(\mathcal{E}, \mathcal{R}) = \left\{ 1 + \left[\frac{R_2(\mathcal{E})}{\mathcal{R}} \right]^n \right\}^{-2/n}. \quad (\text{A2})$$

The flux coefficients, equations (26), are

$$D_{\mathcal{R}} = -\langle \Delta \mathcal{R} \rangle + \frac{1}{2} \frac{\partial}{\partial \mathcal{R}} \langle (\Delta \mathcal{R})^2 \rangle \quad (\text{A3a})$$

$$= 2A(\mathcal{E}) \left[1 + \left(\frac{\mathcal{R}_2}{\mathcal{R}} \right)^n \right]^{-(1+2/n)} \left[1 - 2\mathcal{R} + (3 - 4\mathcal{R}) \left(\frac{\mathcal{R}_2}{\mathcal{R}} \right)^n \right] \\ - 2A(\mathcal{E}) \left[1 + \left(\frac{\mathcal{R}_1}{\mathcal{R}} \right)^n \right]^{-(1+2/n)} \left[1 - 2\mathcal{R} + (3 - 4\mathcal{R}) \left(\frac{\mathcal{R}_1}{\mathcal{R}} \right)^n \right] \quad (\text{A3b})$$

$$D_{\mathcal{R}\mathcal{R}} = \frac{1}{2} \langle (\Delta \mathcal{R})^2 \rangle \quad (\text{A3c})$$

$$= 2A(\mathcal{E}) \mathcal{R} (1 - \mathcal{R}) \left[1 + \left(\frac{\mathcal{R}_2}{\mathcal{R}} \right)^n \right]^{-2/n}. \quad (\text{A3d})$$

It is easy to verify that in this case,

$$D_{\mathcal{R}} = -\langle \Delta \mathcal{R} \rangle + \frac{\langle (\Delta \mathcal{R})^2 \rangle}{2\mathcal{R}} \left[\frac{1 - 2\mathcal{R}}{1 - \mathcal{R}} + \frac{2}{1 + (\mathcal{R}/\mathcal{R}_2)^n} \right]. \quad (\text{A4})$$

In the limit $\mathcal{R} \ll \{\mathcal{R}_1, \mathcal{R}_2\}$, these expressions become

$$D_{\mathcal{R}} \rightarrow 6A(\mathcal{E}) \left[\left(\frac{\mathcal{R}}{\mathcal{R}_2} \right)^2 - \left(\frac{\mathcal{R}}{\mathcal{R}_1} \right)^2 \right], \quad D_{\mathcal{R}\mathcal{R}} \rightarrow 2A(\mathcal{E}) \mathcal{R} \left(\frac{\mathcal{R}}{\mathcal{R}_2} \right)^2. \quad (\text{A5})$$

The \mathcal{R} -directed flux is

$$\phi_{\mathcal{R}} = -D_{\mathcal{R}\mathcal{R}} \frac{\partial f}{\partial \mathcal{R}} - D_{\mathcal{R}} f \quad (\text{A6})$$

which, in the small- \mathcal{R} limit, becomes

$$\phi_{\mathcal{R}} \rightarrow -2A(\mathcal{E}) \left(\frac{\mathcal{R}}{\mathcal{R}_2} \right)^2 \left(3\lambda f + \mathcal{R} \frac{\partial f}{\partial \mathcal{R}} \right), \quad \lambda \equiv 1 - \left(\frac{\mathcal{R}_2}{\mathcal{R}_1} \right)^2. \quad (\text{A7})$$

Steady-state solutions can be characterized by either a constant, or a zero, flux. Setting $\phi_{\mathcal{R}} = 0$ yields

$$f(\mathcal{R}) = f(\mathcal{R}_2) \left(\frac{\mathcal{R}}{\mathcal{R}_2} \right)^{-3\lambda}, \quad \mathcal{R} \ll \{\mathcal{R}_1, \mathcal{R}_2\}. \quad (\text{A8})$$

When $\mathcal{R}_1 < \mathcal{R}_2$, $\lambda < 0$ and the solution decreases toward $\mathcal{R} = 0$; the reverse is true when $\mathcal{R}_1 > \mathcal{R}_2$. Setting $\mathcal{R}_1 = \mathcal{R}_2$ yields $\lambda = 0$ and $f(\mathcal{R}) = \text{const.}$, the “zero-drift” solution.

A steady-state solution with constant but nonzero flux has the small- \mathcal{R} form

$$f(\mathcal{R}) = \left(\frac{\mathcal{R}}{\mathcal{R}_2} \right)^{-2} \left[\frac{1}{2-3\lambda} \frac{\phi_{\mathcal{R}}}{2A} + C_{\lambda} \left(\frac{\mathcal{R}}{\mathcal{R}_2} \right)^{2-3\lambda} \right] \quad (\text{A9})$$

for $\lambda \neq 2/3$, with C_{λ} an integration constant. For $\lambda = 2/3$,

$$f(\mathcal{R}) = \left(\frac{\mathcal{R}}{\mathcal{R}_2} \right)^{-2} \left[-\frac{\phi_{\mathcal{R}}}{2A} \log \left(\frac{\mathcal{R}}{\mathcal{R}_2} \right) + C_{\frac{2}{3}} \right]. \quad (\text{A10})$$

We compute C_{λ} by requiring f to fall to zero at $\mathcal{R} \equiv \mathcal{R}_0$ (“empty loss cone”). The results are

$$f(\mathcal{R}) = f(\mathcal{R}_2) \left(\frac{\mathcal{R}}{\mathcal{R}_2} \right)^{-2} \frac{(\mathcal{R}/\mathcal{R}_0)^q - 1}{(\mathcal{R}_2/\mathcal{R}_0)^q - 1}, \quad q \equiv 2 - 3\lambda, \quad (\text{A11a})$$

$$\phi_{\mathcal{R}}(\mathcal{E}) = -2qA(\mathcal{E}) \frac{f(\mathcal{R}_2)}{1 - (\mathcal{R}_2/\mathcal{R}_0)^q} \quad (\text{A11b})$$

for $\lambda \neq 2/3$, and

$$f(\mathcal{R}) = f(\mathcal{R}_2) \left(\frac{\mathcal{R}}{\mathcal{R}_2} \right)^{-2} \frac{\log(\mathcal{R}/\mathcal{R}_0)}{\log(\mathcal{R}_2/\mathcal{R}_0)}, \quad (\text{A12a})$$

$$\phi_{\mathcal{R}}(\mathcal{E}) = -2A(\mathcal{E}) \frac{f(\mathcal{R}_2)}{\log(\mathcal{R}_2/\mathcal{R}_0)} \quad (\text{A12b})$$

for $\lambda = 2/3$.

At most energies, $\mathcal{R}_0 \ll \mathcal{R}_2$. Assuming this inequality, f and $\phi_{\mathcal{R}}$ have the following forms, depending on the value of λ :

1. $\lambda > 2/3$, i.e. $\mathcal{R}_1/\mathcal{R}_2 > \sqrt{3}$. Defining $p \equiv 3\lambda - 2 > 0$,

$$\frac{f(\mathcal{R})}{f(\mathcal{R}_2)} \approx \left(\frac{\mathcal{R}_2}{\mathcal{R}} \right)^2 \left[1 - \left(\frac{\mathcal{R}_0}{\mathcal{R}} \right)^p \right], \quad \phi_{\mathcal{R}} \approx -2pA(\mathcal{E})f(\mathcal{R}_2). \quad (\text{A13})$$

2. $\lambda < 2/3$, i.e. $\mathcal{R}_1/\mathcal{R}_2 < \sqrt{3}$. In terms of $q \equiv 2 - 3\lambda > 0$,

$$\frac{f(\mathcal{R})}{f(\mathcal{R}_2)} \approx \left(\frac{\mathcal{R}_2}{\mathcal{R}} \right)^2 \left[\left(\frac{\mathcal{R}}{\mathcal{R}_2} \right)^q - \left(\frac{\mathcal{R}_0}{\mathcal{R}_2} \right)^q \right], \quad \phi_{\mathcal{R}} \approx -2qA(\mathcal{E}) \left(\frac{\mathcal{R}_0}{\mathcal{R}_2} \right)^q f(\mathcal{R}_2). \quad (\text{A14})$$

The “zero-drift” case has $\mathcal{R}_1 = \mathcal{R}_2$, $\lambda = 0$, $q = 2$.

3. $\lambda = 2/3$, i.e. $\mathcal{R}_1/\mathcal{R}_2 = \sqrt{3}$:

$$\frac{f(\mathcal{R})}{f(\mathcal{R}_2)} \approx \left(\frac{\mathcal{R}_2}{\mathcal{R}} \right)^2 \frac{\log(\mathcal{R}/\mathcal{R}_0)}{\log(\mathcal{R}_2/\mathcal{R}_0)}, \quad \phi_{\mathcal{R}} \approx -\frac{2A(\mathcal{E})f(\mathcal{R}_2)}{\log(\mathcal{R}_2/\mathcal{R}_0)}. \quad (\text{A15})$$

It is interesting to compare the expressions for the flux to those that would obtain in the absence of anomalous relaxation. Repeating the analysis with $g_1 = g_2 = 1$, we find:

$$D_{\mathcal{R}} = 0, \quad D_{\mathcal{R}\mathcal{R}} = 2A(\mathcal{E})\mathcal{R}(1 - \mathcal{R}), \quad \phi_{\mathcal{R}} = -2A(\mathcal{E})\mathcal{R}(1 - \mathcal{R}) \frac{\partial f}{\partial \mathcal{R}}, \quad (\text{A16})$$

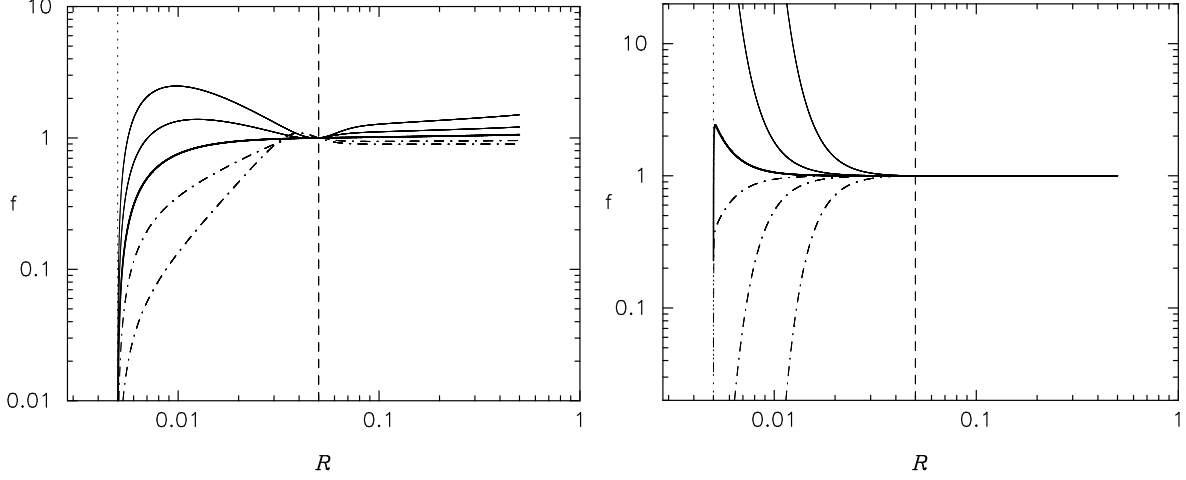


FIG. 10.— Steady-state solutions in the anomalous-relaxation regime, under two assumptions about how the resonant diffusion coefficients are modified. **Left panel:** Power-law modification, equations (A2), with $n = 8$, $\mathcal{R}_2 = 0.05$ (shown by the vertical dashed line), and boundary condition $f(\mathcal{R}) = 0$ at $\mathcal{R} = 0.005$ (show by the vertical dotted line). $\mathcal{R}_1/\mathcal{R}_2 = \{0.8, 0.9, 1, 1.1, 1.25\}$. Solid lines: $\mathcal{R}_1/\mathcal{R}_2 \geq 1$; dot-dashed lines: $\mathcal{R}_1/\mathcal{R}_2 < 1$. **Right panel:** Exponential modification, equations (A23), with $\mathcal{R}_4 = 0.05$ and $\mathcal{R}_3/\mathcal{R}_4 = \{0.99, 0.999, 0.9999, 1.0001, 1.001, 1.01\}$. Solid lines: $\mathcal{R}_3/\mathcal{R}_4 > 1$; dot-dashed lines: $\mathcal{R}_3/\mathcal{R}_4 < 1$.

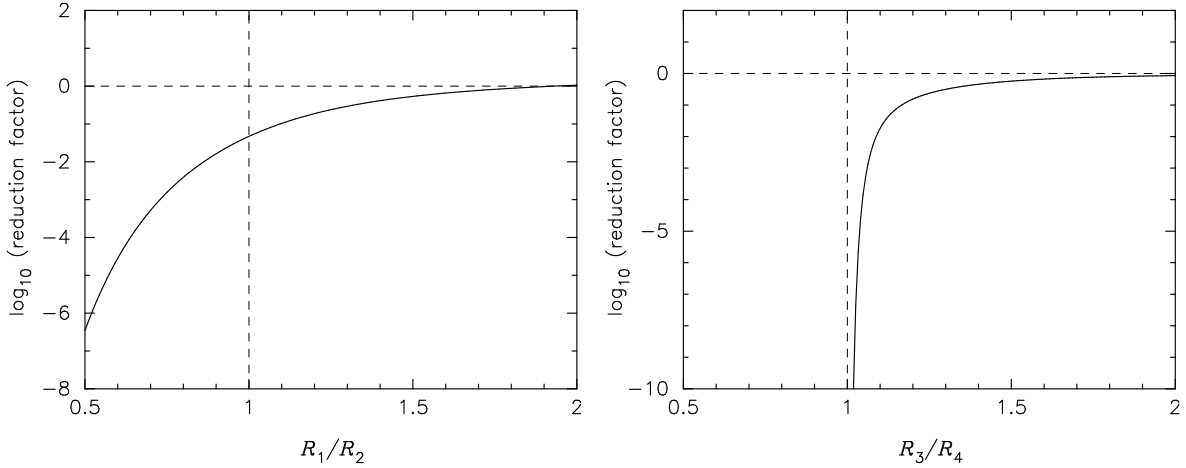


FIG. 11.— Reduction in the steady-state flux due to anomalous diffusion. **Left panel:** power-law modification; **right panel:** exponential modification. Both curves assume $f(\mathcal{R}) = 0$ at $\mathcal{R} = 0.005$, as in Figure 10.

so that the steady state is characterized by

$$2A(\mathcal{E})\mathcal{R}(1-\mathcal{R})\frac{\partial f}{\partial \mathcal{R}} + \phi_{\mathcal{R}} = 0. \quad (\text{A17})$$

The solution is

$$\frac{f(\mathcal{R})}{f(\mathcal{R}_2)} = \frac{\log\left(\frac{\mathcal{R}}{1-\mathcal{R}}\right) - \log\left(\frac{\mathcal{R}_0}{1-\mathcal{R}_0}\right)}{\log\left(\frac{\mathcal{R}_2}{1-\mathcal{R}_2}\right) - \log\left(\frac{\mathcal{R}_0}{1-\mathcal{R}_0}\right)} \quad (\text{A18})$$

with flux

$$\phi_{\mathcal{R}} = -2A(\mathcal{E})\frac{f(\mathcal{R}_2)}{\log\left(\frac{\mathcal{R}_2}{1-\mathcal{R}_2}\right) - \log\left(\frac{\mathcal{R}_0}{1-\mathcal{R}_0}\right)} \quad (\text{A19})$$

Again supposing that $\mathcal{R}_0 \ll \mathcal{R}_2$, these expressions become:

$$\frac{f(\mathcal{R})}{f(\mathcal{R}_2)} \approx \frac{\log \mathcal{R} - \log \mathcal{R}_0}{\log \mathcal{R}_2 - \log \mathcal{R}_0}, \quad \phi_{\mathcal{R}} \approx -\frac{2A(\mathcal{E})f(\mathcal{R}_2)}{\log(\mathcal{R}_2/\mathcal{R}_0)}. \quad (\text{A20})$$

Define a “reduction factor,” η , as the ratio of this flux to the flux that would obtain in the presence of anomalous

relaxation, assuming the same value for $f(\mathcal{R}_2)$. Then

$$\eta \approx \begin{cases} p \log(\mathcal{R}_2/\mathcal{R}_0) & \text{if } \mathcal{R}_1/\mathcal{R}_2 > \sqrt{3} \\ q(\mathcal{R}_0/\mathcal{R}_2)^q \log(\mathcal{R}_2/\mathcal{R}_0) & \text{if } \mathcal{R}_1/\mathcal{R}_2 < \sqrt{3} \\ 1 & \text{if } \mathcal{R}_1/\mathcal{R}_2 = \sqrt{3}. \end{cases}$$

Figures 10 and 11 plot more accurate expressions for $f(\mathcal{R})$ and η , computed using equations (A3) and (A6), without assuming the smallness of \mathcal{R} or \mathcal{R}_0 .

The “zero-drift” solution has $\mathcal{R}_1 = \mathcal{R}_2$, $\lambda = 0$ and $q = 2$. For these values,

$$\eta = 2 \left(\frac{\mathcal{R}_0}{\mathcal{R}_2} \right)^2 \log \left(\frac{\mathcal{R}_2}{\mathcal{R}_0} \right). \quad (\text{A21})$$

For $\mathcal{R}_0/\mathcal{R}_2 = \{0.5, 0.1, 0.01, 0.001\}$, $\eta \approx \{0.35, 0.046, 9.2 \times 10^{-4}, 1.4 \times 10^{-5}\}$.

The value of $\mathcal{R}_1/\mathcal{R}_2$ favored in the numerical experiments was ~ 0.8 , implying $\lambda \approx -0.56$ and $q \approx 3.7$. For these values,

$$\eta \approx 3.7 \left(\frac{\mathcal{R}_0}{\mathcal{R}_2} \right)^{3.7} \log \left(\frac{\mathcal{R}_2}{\mathcal{R}_0} \right). \quad (\text{A22})$$

For $\mathcal{R}_0/\mathcal{R}_2 = \{0.5, 0.1, 0.01, 0.001\}$, $\eta \approx \{0.20, 1.7 \times 10^{-3}, 6.8 \times 10^{-7}, 2.0 \times 10^{-10}\}$.

(2) Exponential

Next we identify $\{w_1, w_2\}$ with $\{h_1, h_2\}$ given by equations (42) and (41):

$$\begin{aligned} h_1(\mathcal{E}, \mathcal{R}) &= \left[1 + \frac{2(1-\mathcal{R})}{1-2\mathcal{R}} \left(\frac{\mathcal{R}_3}{\mathcal{R}} \right)^2 \right] \exp \left(-\frac{\mathcal{R}_3^2}{\mathcal{R}^2} \right), \\ h_2(\mathcal{E}, \mathcal{R}) &= \exp \left(-\frac{\mathcal{R}_4^2}{\mathcal{R}^2} \right). \end{aligned} \quad (\text{A23})$$

The flux coefficients are

$$\begin{aligned} D_{\mathcal{R}} &= 2A(\mathcal{E}) \left[1 - 2\mathcal{R} + 2(1-\mathcal{R}) \left(\frac{\mathcal{R}_4}{\mathcal{R}} \right)^2 \right] \exp \left(-\frac{\mathcal{R}_4^2}{\mathcal{R}^2} \right) \\ &\quad - 2A(\mathcal{E}) \left[1 - 2\mathcal{R} + 2(1-\mathcal{R}) \left(\frac{\mathcal{R}_3}{\mathcal{R}} \right)^2 \right] \exp \left(-\frac{\mathcal{R}_3^2}{\mathcal{R}^2} \right), \end{aligned} \quad (\text{A24a})$$

$$D_{\mathcal{R}\mathcal{R}} = 2A(\mathcal{E})\mathcal{R}(1-\mathcal{R}) \exp \left(-\frac{\mathcal{R}_4^2}{\mathcal{R}^2} \right) \quad (\text{A24b})$$

and

$$D_{\mathcal{R}} = -\langle \Delta \mathcal{R} \rangle + \frac{\langle (\Delta \mathcal{R})^2 \rangle}{2\mathcal{R}} \left(\frac{1-2\mathcal{R}}{1-\mathcal{R}} + 2\frac{\mathcal{R}_4^2}{\mathcal{R}^2} \right). \quad (\text{A25})$$

In the limit $\mathcal{R} \ll \{\mathcal{R}_3, \mathcal{R}_4\}$, these expressions become

$$D_{\mathcal{R}} \rightarrow 4A(\mathcal{E}) \left(\frac{\mathcal{R}_4}{\mathcal{R}} \right)^2 \exp \left(-\frac{\mathcal{R}_4^2}{\mathcal{R}^2} \right) \left[1 - \frac{\mathcal{R}_3^2}{\mathcal{R}_4^2} \exp \left(-\frac{\mathcal{R}_3^2 - \mathcal{R}_4^2}{\mathcal{R}^2} \right) \right], \quad D_{\mathcal{R}\mathcal{R}} \rightarrow 2A(\mathcal{E})\mathcal{R} \exp \left(-\frac{\mathcal{R}_4^2}{\mathcal{R}^2} \right). \quad (\text{A26})$$

In the same limit, the \mathcal{R} -directed flux is

$$\phi_{\mathcal{R}} \rightarrow -2A(\mathcal{E}) \exp \left(-\frac{\mathcal{R}_4^2}{\mathcal{R}^2} \right) \left\{ 2 \left(\frac{\mathcal{R}_4}{\mathcal{R}} \right)^2 \left[1 - \frac{e^{-\delta \mathcal{R}_3^2/\mathcal{R}^2}}{1-\delta} \right] f + \mathcal{R} \frac{\partial f}{\partial \mathcal{R}} \right\}, \quad \delta \equiv 1 - \left(\frac{\mathcal{R}_4}{\mathcal{R}_3} \right)^2. \quad (\text{A27})$$

Setting $\phi_{\mathcal{R}} = 0$ yields

$$\frac{\log f(\mathcal{R})}{\log f(\mathcal{R}_4)} = \frac{\mathcal{R}_4^2}{\mathcal{R}^2} - 1 + \frac{\mathcal{R}_3^2}{\mathcal{R}_3^2 - \mathcal{R}_4^2} \left[\exp \left(\frac{\mathcal{R}_4^2 - \mathcal{R}_3^2}{\mathcal{R}^2} \right) - \exp \left(\frac{\mathcal{R}_4^2 - \mathcal{R}_3^2}{\mathcal{R}_4^2} \right) \right], \quad \mathcal{R} \ll \{\mathcal{R}_3, \mathcal{R}_4\}. \quad (\text{A28})$$

For $\mathcal{R}_3 < \mathcal{R}_4$, the dominant terms imply

$$f(\mathcal{R}) \rightarrow f(\mathcal{R}_4) \exp \left[\delta^{-1} \exp \left(\alpha \frac{\mathcal{R}_4^2}{\mathcal{R}^2} \right) \right] \quad (\text{A29})$$

where $\delta = 1 - \mathcal{R}_4^2/\mathcal{R}_3^3 < 0$, $\alpha = 1 - \mathcal{R}_3^2/\mathcal{R}_4^2 > 0$, hence f drops very rapidly to zero below $\mathcal{R} = \mathcal{R}_4$. Whereas for $\mathcal{R}_3 > \mathcal{R}_4$,

$$f(\mathcal{R}) \rightarrow f(\mathcal{R}_4)e^{\mathcal{R}_4^2/\mathcal{R}^2}, \quad (\text{A30})$$

a rapid rise toward $\mathcal{R} = 0$. This is qualitatively the same behavior as in the power-law case when $\phi_{\mathcal{R}} = 0$.

In the case of a constant but nonzero flux, only the “zero-drift” solution (with $\mathcal{R}_3 = \mathcal{R}_4$) can be expressed in terms of simple functions:

$$f(\mathcal{R}) \approx -\frac{\phi_{\mathcal{R}}}{4A} \left[E_i \left(\frac{\mathcal{R}_4^2}{\mathcal{R}_0^2} \right) - E_i \left(\frac{\mathcal{R}_4^2}{\mathcal{R}^2} \right) \right], \quad \mathcal{R} \ll \mathcal{R}_3, \mathcal{R}_4 \quad (\text{A31a})$$

$$\frac{f(\mathcal{R})}{f(\mathcal{R}_4)} \approx \frac{E_i(\mathcal{R}_4^2/\mathcal{R}_0^2) - E_i(\mathcal{R}_4^2/\mathcal{R}^2)}{E_i(\mathcal{R}_4^2/\mathcal{R}_0^2) - E_i(1)}, \quad (\text{A31b})$$

$$-\frac{\phi_{\mathcal{R}}}{4A} \approx f(\mathcal{R}_4) \left[E_i \left(\frac{\mathcal{R}_4^2}{\mathcal{R}_0^2} \right) - E_i(1) \right]^{-1}. \quad (\text{A31c})$$

In these expressions, E_i is the exponential function. The reduction factor defined above becomes, in this case,

$$\eta = 2 \frac{\mathcal{R}_4}{\mathcal{R}_0} \log \left(\frac{\mathcal{R}_4}{\mathcal{R}_0} \right) e^{-\mathcal{R}_4/\mathcal{R}_0} \quad (\text{A32})$$

For $\mathcal{R}_0/\mathcal{R}_4 = \{0.5, 0.1, 0.01\}$, $\eta \approx \{0.38, 2.1 \times 10^{-3}, 3.4 \times 10^{-41}\}$.

REFERENCES

- Antonini, F., & Merritt, D. 2012, ApJ, 745, 83
 Antonini, F., & Merritt, D. 2013, ApJ, 763, LL10
 Bahcall, J. N., & Wolf, S. 1976, ApJ, 209, 214
 Bahcall, J. N., & Wolf, R. A. 1977, ApJ, 216, 883
 Bar-Or, B., & Alexander, T. 2014, Classical and Quantum Gravity, 31, 244003
 Bartko, H., et al. 2010, ApJ, 708, 834
 Begelman, M. C., Blandford, R. D., & Rees, M. J. 1980, Nature, 287, 307
 Brem, P., Amaro-Seoane, P., & Sopena, C. F. 2014, MNRAS, 437, 1259
 Buchholz, R. M., Schödel, R., & Eckart, A. 2009, A&A, 499, 483
 Chandrasekhar, S. 1942, The Principles of Stellar Dynamics. Chicago, The University of Chicago press.
 Chatzopoulos, S., Fritz, T. K., Gerhard, O., et al. 2015, MNRAS, 447, 952
 Cohn, H. & Kulsrud, R. 1978, ApJ, 226, 1087
 Do, T., Ghez, A. M., Morris, M. R., Lu, J. R., Matthews, K., Yelda, S., & Larkin, J. 2009, ApJ, 703, 1323
 Do, T., Martinez, G. D., Yelda, S., et al. 2013, ApJ, 779, L6
 Eilon, E., Kupa, G., & Alexander, T. 2009, ApJ, 698, 641
 Freitag, M., Amaro-Seoane, P., & Kalogera, V. 2006, ApJ, 649, 91
 Gürkan, M. A., & Hopman, C. 2007, MNRAS, 379, 1083
 Hamers, A., Portegies Zwart, S. & Merritt, D. 2014, MNRAS, in press
 Hénon, M. 1961, Annales d’Astrophysique, 24, 369
 Hopman, C. 2009, Classical and Quantum Gravity, 26, 094028
 Hopman, C., & Alexander, T. 2006, ApJ, 645, L133
 Hopman, C., & Alexander, T. 2006, ApJ, 645, L133
 Lee, E. P. 1969, ApJ, 155, 687
 Madigan, A.-M., Hopman, C., & Levin, Y. 2011, ApJ, 738, 99
 Magorrian, J. & Tremaine, S. 1998, MNRAS, 309, 447.
 Merritt, D. 2009, ApJ, 694, 959
 Merritt, D. 2010, ApJ, 718, 739
 Merritt, D. 2013, Dynamics and Evolution of Galactic Nuclei (Princeton: Princeton University Press).
 Merritt, D. 2015a, ApJ, 804:52 (Paper I)
 Merritt, D. 2015b, ApJ, 804:128 (Paper II)
 Merritt, D. 2015c, ApJ, in press (Paper IV)
 Merritt, D., Alexander, T., Mikkola, S., & Will, C. M. 2010, Phys. Rev. D, 81, 062002
 Merritt, D., Alexander, T., Mikkola, S., & Will, C. M. 2011, Phys. Rev. D, 84, 044024
 Merritt, D., Antonini, F., & Vasiliev, E. 2015, submitted to *The Astrophysical Journal*
 Merritt, D., Storch-Bergmann, T., Robinson, A., et al. 2006, MNRAS, 367, 1746
 Merritt, D., & Szell, A. 2006, ApJ, 648, 890
 Merritt, D., & Wang, J. 2005, ApJ, 621, L101
 Milosavljević, M., & Merritt, D. 2001, ApJ, 563, 34
 Milosavljević, M., & Merritt, D. 2003, ApJ, 596, 860
 Merritt, D., & Vasiliev, E. 2012, Phys. Rev. D, 86, 102002
 Rauch, K. P., & Tremaine, S. 1996, New Astron., 1, 149
 Rosenbluth, M. N., MacDonald, W. M., & Judd, D. L. 1957, Physical Review, 107, 1
 Schödel, R. 2011, Highlights of Spanish Astrophysics VI, 36
 Schödel, R., Merritt, D., & Eckart, A. 2009, A&A, 502, 91
 Sigurdsson, S., & Rees, M. J. 1997, MNRAS, 284, 318